

**Forschungszentrum Karlsruhe**  
Technik und Umwelt

**Wissenschaftliche Berichte**

FZKA 6010

**Turbulent Rayleigh-Bénard  
Convection in  
Low Prandtl-number Fluids**

**S. Horanyi, L. Krebs, U. Müller**

**Institut für Angewandte Thermo- und Fluidodynamik**

**Februar 1998**

---



**FORSCHUNGSZENTRUM KARLSRUHE**  
Technik und Umwelt  
Wissenschaftliche Berichte  
FZKA 6010

# **Turbulent Rayleigh-Bénard Convection in Low Prandtl-number Fluids**

**S. Horanyi, L. Krebs, U. Müller**

Institut für Angewandte Thermo- und Fluidodynamik

Forschungszentrum Karlsruhe GmbH, Karlsruhe  
1998

**Als Manuskript gedruckt  
Für diesen Bericht behalten wir uns alle Rechte vor**

**Forschungszentrum Karlsruhe GmbH  
Postfach 3640, 76021 Karlsruhe**

**Mitglied der Hermann von Helmholtz-Gemeinschaft  
Deutscher Forschungszentren (HGF)**

**ISSN 0947-8620**

## Abstract

An experimental investigation of Rayleigh-Bénard convection in liquid sodium has been performed in cylindrical test cells with aspect ratios between 20 and 4.6 for a range of Rayleigh numbers  $10^4 < Ra < 5 \cdot 10^6$ . The Prandtl number is between  $6.0 \cdot 10^{-2} \pm 0.1 \cdot 10^{-3}$ . For low Rayleigh number  $Ra < 10^4$  the dimensionless heat flux,  $Nu$ , is mainly conduction controlled and close to 1; a correlation  $Nu = 0.115 Ra^{0.25}$  describes the observations adequately for  $2 \cdot 10^4 < Ra < 5 \cdot 10^6$ . It is shown that the Nusselt numbers are smaller for sodium than for other fluids with larger Prandtl numbers such as mercury and helium. This contrasts with the relation  $Nu \sim (Ra^{2/7} \cdot Pr^{-1/7})$  but conforms with the theoretically predicted relation  $Nu \sim (RaPr)^{1/4}$  for low Prandtl number fluids. The heat transfer as well as the statistical properties of the turbulent convection are significantly influenced by convection mode transitions in the test cell of small aspect ratio. The formation of thermal boundary layers occurs only at high Rayleigh numbers of the order  $Ra > 10^6$ . An instability in these thermal boundary layer triggers a new mode of large scale fluctuating motion. The analysis of the temperature time signals shows that the temperature field behaviour up to a Rayleigh number  $Ra \sim 5 \cdot 10^6$  is essentially dissipative.

## Turbulente Rayleigh-Bénard Konvektion in Flüssigkeiten mit niedrigen Prandtl-Zahlen

### Zusammenfassung

Eine Rayleigh-Bénard Konvektionsströmung in flüssigem Natrium wurde in zylindrischen Behältern mit einem Durchmesser- zu Höhenverhältnis zwischen 20 und 4.6 in einem Bereich der Rayleigh-Zahlen von  $10^4 < Ra < 5 \cdot 10^6$  untersucht. Die Prandtl-Zahl betrug dabei  $6.0 \cdot 10^{-3} \pm 0.1 \cdot 10^{-3}$ . Für kleine Rayleigh-Zahlen  $Ra < 10^4$  ist der Wärmefluß über die Schicht im wesentlichen durch Wärmeleitung bestimmt. Die Nusselt-Zahl liegt dann nahe bei dem Wert eins. Im Bereich der Rayleigh-Zahlen von  $2 \cdot 10^4 < Ra < 5 \cdot 10^6$  beschreibt eine Beziehung  $Nu = 0.115 \cdot Ra^{0.25}$  die experimentellen Daten für den Wärmedurchgang zufriedenstellend. Es kann gezeigt werden, daß die Nusselt-Zahlen für flüssige Natriumschichten kleiner ausfallen als für jede andere Flüssigkeit mit größeren Prandtl-Zahlen wie etwa Quecksilber oder Helium. Dies ist in Widerspruch zur theoretisch herleitbaren Beziehung  $Nu \sim (Ra^{2/7} \cdot Pr^{-1/7})$ , stimmt aber für kleine Prandtl-Zahlen mit der Relation  $Nu \sim (RaPr)^{1/4}$  überein. Die Wärmeübertragung und die statistischen Eigenschaften der turbulenten Konvektion werden wesentlich bestimmt durch Übergänge zwischen verschiedenen Konvektionsmoden in einem Versuchsbehälter mit relativ kleinem Durchmesser- zu Höhenverhältnis. Thermische Grenzschichten bilden sich erst bei hohen Rayleigh-Zahlen der Ordnung  $Ra > 10^6$  aus. Eine Instabilität dieser thermischen Grenzschicht scheint eine neue großräumige zeitlich fluktuierende Konvektionsform auszulösen. Die Analyse der zeitabhängigen Temperatursignale zeigt, daß sich die Temperatur im untersuchten Rayleigh-Zahl-Bereich wie ein passiver Skalar verhält.

## Contents

1.	Introduction .....	1
2.	Brief survey of the literature .....	2
3.	The experimental set up, measuring technique and data evaluation .....	4
4.	Results .....	8
4.1	General observations .....	8
4.2	The dimensionless heat transfer $Nu(Ra)$ .....	11
4.3	Axial mean temperature profiles in the sodium layer .....	14
4.4	Evaluation of temperature fluctuation signals .....	16
5.	Discussion and Conclusions .....	27

## 1. Introduction

An improved understanding of turbulent free convection in liquids of very low Prandtl number (i. e. high thermal conductivity) such as liquid metals and other high temperature molten materials is highly desirable for several applications in nuclear power engineering and more recently in materials processing industries. It is equally important for explaining and modeling certain geo-planetary or astrophysical observations for instance the granular structure of the solar surface or planetary or stellar magnetic fields. A well defined and experimentally accessible free convection system is the Rayleigh-Benard-convection in plane horizontal liquid layers with large temperature differences between top and bottom. In recent years several novel experiments have been conducted in high Rayleigh-Bénard convection by different research groups (see Castaing et. al. (1989); Heslot et al. (1987); Tilgner et. al. (1993); Salomon and Gollub (1990); Cioni et. al. (1996); Krishnamurti (1995); Goldstein et. al. (1990)). Most of these experiments were performed in containers with an aspect ratio one and with either water or helium as test fluids whose Prandtl numbers are  $Pr \approx 7$  and  $0.7$  respectively. Only Cioni et. al. (1995) and Takeshita et al. (1996) report experiments in mercury with  $Pr \approx 0.025$ . The new experiments have, on the one hand, advanced the available heat transfer data base into the very high Rayleigh number regime,  $Ra < 10^{15}$  and, moreover, provided new local mean and statistical data of the temperature and velocity field of buoyant turbulent flows. On the other hand they have initiated modelling efforts for turbulent flow which center around modifications of scaling laws for heat transfer and spectral dynamics of the temperature due to the interaction of large scale "cellular" motion and small scale turbulence in sheared thermal boundary layers (see Castaing et. al. (1989), Yakot (1989), Shraiman and Siggia (1990) Wu et. al. (1990), Chilla et. al. 1993)). New concepts such as "soft" and "hard" turbulence have been introduced based on the structure of the probability density function measured in test containers of small height to diameter ratio and at high Rayleigh numbers (Castaing et. al. (1989)) and new "structure" functions were proposed to characterize the intermittent behaviour of turbulent flows. We believe that the new experimental and theoretical approach to thermal turbulence needs completion if not correction with regard to the influence of low Prandtl number and aspect ratio. We therefore resumed the former experimental work of Kek (1989) on heat transfer through liquid sodium layers and have extended the previous investigations to a Rayleigh number range  $2.5 \cdot 10^5 < Ra < 4.5 \cdot 10^6$ . The new experiments were performed in cylindrical containers of aspect ratio, diameter to height of 20 and 4.6.

This paper presents new data for the heat transfer through sodium layers and for the time averaged temperature distribution across the layer. Furthermore, statistical data of temperature signals are presented and discussed such as root mean square values (RMS), probability density functions (PDF) and power spectrum density functions (PSD) for different heating powers. Data from cross correlation measurements between temperature probes provide a clue about the buoyant velocity in the layer.

## 2. Brief survey of the literature

An extensive survey of the current state of knowledge on turbulent Bénard convection has been compiled by Siggia (1994). A summary of the empirical and theoretical heat transfer correlations applicable for low Prandtl number convection has been given by Kek and Müller (1993). Here, we list in Table 1 some frequently used heat transfer correlations applicable to low Prandtl number flow.

$Nu = 0.069 Ra^{0.33} Pr^{0.074}$	$1.5 \cdot 10^5 < Ra < 4 \cdot 10^7$ (for any fluid)	Globe and Dropkin (1959);
$Nu = 0.147 Ra^{0.257}$	$10^3 < Ra < 5 \cdot 10^5$ (mercury)	Rosby (1969);
$Nu = 0.078 Ra^{0.32}$	$4.8 \cdot 10^6 < Ra < 4 \cdot 10^7$ (sodium)	Mc Donald, Connoly (1960);
$Nu = 0.140 Ra^{0.26}$	$4.6 \cdot 10^6 < Ra < 4.5 \cdot 10^8$ (mercury)	} Cioni et al. (1996);
$Nu = 0.44 Ra^{0.20}$	$4.5 \cdot 10^8 < Ra < 2.1 \cdot 10^9$ (mercury)	
$Nu = 0.155 Ra^{0.27}$	$2 \cdot 10^6 < Ra < 8 \cdot 10^7$ (mercury)	Takeshita et al. (1996);
model correlations:		
$Nu = 0.17 (RaPr)^{1/3}$	$Ra \gg 1700, Pr \ll 1$	Kraichnan (1962);
$Nu = 0.175 Ra^{1/4}$	$[Ra \cdot Pr]^{1/2} \gg 1$	Busse and Clever (1981)
$Nu = 0.27 Ra^{2/7} \cdot Pr^{-1/7}$	$(10^7 - 10^8) Pr^{3/5} < Ra < (10^{13} - 10^{15}) Pr^4$	Shraiman and Siggia (1990)
$Nu = 0.25 (RaPr)^{2/7}$	$10^6 < Ra < 10^9$	Cioni et al. (1996)

**Table 1. Heat Transfer correlations and Range of Validity.**



It has been debated by several research groups whether the heat transfer correlation in form of the  $1/3$  power law describes the experimental observations properly within the experimental error bounds or whether a power of  $2/7 \approx 0.286$  applies as derived by Castaing et al. (1989). It is not obvious a priori why careful measurements in water conducted by Krishnamurti (1994) and by Goldstein et al. (1990) do not confirm strictly the  $Nu \sim Ra^{2/7}$  power law observed in experiments by Heslot et al. (1987) in helium and by Cioni et al. (1996) in water and mercury. But there is significant evidence from the experimental findings of Krishnamurti, that the realized different large scale convection patterns in the test cells of different experimenters give rise to the discrepancies in the heat transfer correlations.

Moreover, it is evident that the correlation of Shraiman & Siggia (1990) in table 1 fails to predict properly the heat transfer for very low values of the Prandtl number because of its singular behaviour for  $Pr \rightarrow 0$ . As the range of application in their derivation depends on positive powers of  $Pr$ , it would shrink to zero for  $Pr \rightarrow 0$ . This clearly indicates the limited validity of the underlying physical conception.

Temperature distributions across the layer height in turbulent convection have been measured repeatedly in the past in air, water and silicon oil by Deardorf and Willis (1966, 1967). Goldstein and Chu (1969, 1973), Somerscales and Gazda (1969). Velocity measurements for very high Rayleigh number flow are scarce. To our knowledge only mean velocity profile have been measured by Garon and Goldstein (1973), Kikuchi et al. (1986) and Tilgner et al. (1993). In a few cases local mean velocities at the layer mid-height have been obtained by temperature correlation measurements or particle image velocimetry in helium and water see, for example Tanaka and Miyata (1980), Sano et al (1989). Statistical properties of turbulent convection are available from several research groups for air, helium and water. Here, the data for the temperature field are far more complete than those for the velocity field. RMS-values and distributions as well as power density spectra for the temperature and velocity in air field have been given by Deardorf and Willis (1967) in an intermediate range of Rayleigh numbers,  $6.3 \cdot 10^5 < Ra < 1.0 \cdot 10^7$ . For water and for one particular value  $Ra = 1.1 \cdot 10^9$ . Tilgner et al. (1993) have obtained RMS-values for the temperature and velocity field in the vicinity of the cooled upper boundary. Power density spectra (PDS) and probability density functions (PDF) of the temperature time signals have been provided for the test fluid helium and a wide range of Rayleigh numbers by Libchaber and his group

(Heslot, Castaing, Libchaber (1987), Sano, Wu, Libchaber (1989)). Their measurements have initiated a sequel of theoretical research activities in the field of highly turbulent convection. A particular new phenomenon is the observed transition of the probability density functions for temperature from a Gaussian distribution to an exponential one in convection experiments at very high Rayleigh numbers. After Castaing et al. (1989) the related turbulent flow field is termed either "soft" or "hard" respectively.

Compared with the available experimental investigations in fluids of moderate Prandtl numbers the data base for statistical evaluations of turbulent flow from experiments in liquid metals is very limited. A first attempt to evaluate temperature time signals from mercury experiments in terms of power density spectra was undertaken by Rossby (1969). Recently some more investigations were performed by Kek (1989), Cioni (1993), Cioni et. al. (1995) and Takeshita et al. (1996) who provide data such as the temperature variance, the skewness and flatness, the probability density function and power density spectra employing time signals measurements with thermocouples inside the layer. Kek performed his measurements in liquid sodium in a relatively low Rayleigh number range  $Ra < 2.4 \cdot 10^5$  while Cioni's mercury data apply for  $4.6 \cdot 10^6 < Ra < 6.3 \cdot 10^9$  and Takeshita's for  $10^6 < Ra < 10^8$ . There are in general only very few measurements available for free convection in low Prandtl number fluids, which encouraged us to continue the sodium experiments first started by Kek (1982, 1989).

### 3. The experimental set up, measuring technique and data evaluation

The convection apparatus and the measuring technique have been described elsewhere in detail, Kek and Mueller (1993). We therefore limit ourselves to outline the essential features only. The test apparatus is depicted schematically in Fig. 1. The dimensions of the circular test chamber are 500 mm in diameter and 15.5, 25, 40 and 110 mm in height. Most of the new experiments are conducted with a layer height of 110 mm. The experiments are carried out at a mean temperature level between 550 - 570 K in the sodium and for heating powers of 1 to 17 kW at the bottom plate. The temperature of the cooling plate is kept constant, using a boiling cooler and oil as a coolant. The temperature difference is measured across the sodium layer by 6 pairs of Pt-100 resistance thermometers placed in bore holes which are radially drilled into the top and bottom copper plates of the test apparatus at different depth. Two rakes equipped with 9 thermocouples each at different vertical elevations are placed near the center of

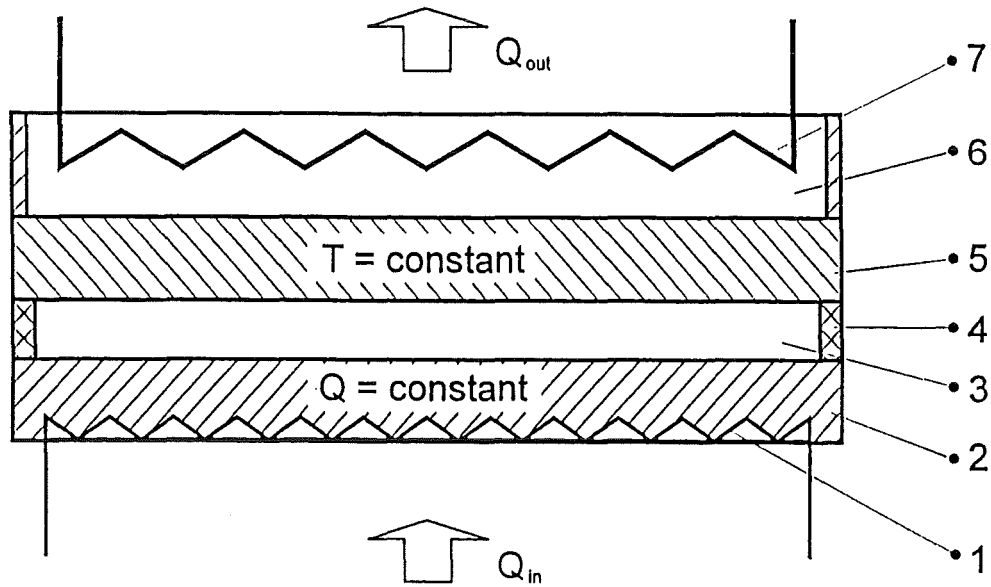


Fig. 1: Schematic sketch of the test apparatus; electrical power supply (1), heating plate, copper (2) sodium layer (3), side wall, nickel (4), cooling plate, copper (5), boiling cooler, oil (6), heat exchanger, water/oil (7)

the test cell to measure the vertical temperature profile in the layer. A sketch of the resistance thermometers, the thermocouple rake and their location is shown in Figs. 2a, b. In order to control the uniformity of the test section temperature, 9 more thermocouples are located at the perimeter of the test section in three sets, each consisting of three thermocouples, fixed in a  $120^\circ$  subdivision on the side wall of the container. The thermocouples in each set are arranged in a vertical line at intervals of 3 cm. In addition, a prong fitted with 8 thermocouples at particular positions and at equal distances from each other was moved repeatedly during the test runs into the center bore hole of the cooling plate to measure the local temperature distribution of the upper boundary along radius. Also, during the experiments all the Pt-100 resistance thermometers were repeatedly moved radially in their particular bore holes to selected radial positions to check the temperature uniformity of the upper and lower boundaries in the azimuthal direction.

The integral properties of the test, the Rayleigh number  $Ra$ , the mean heat transfer coefficient  $\bar{\alpha}$  and the mean Nusselt number  $\bar{Nu}$  are evaluated in the same manner as in the paper by Kek and Müller (1993). The following definitions are used:

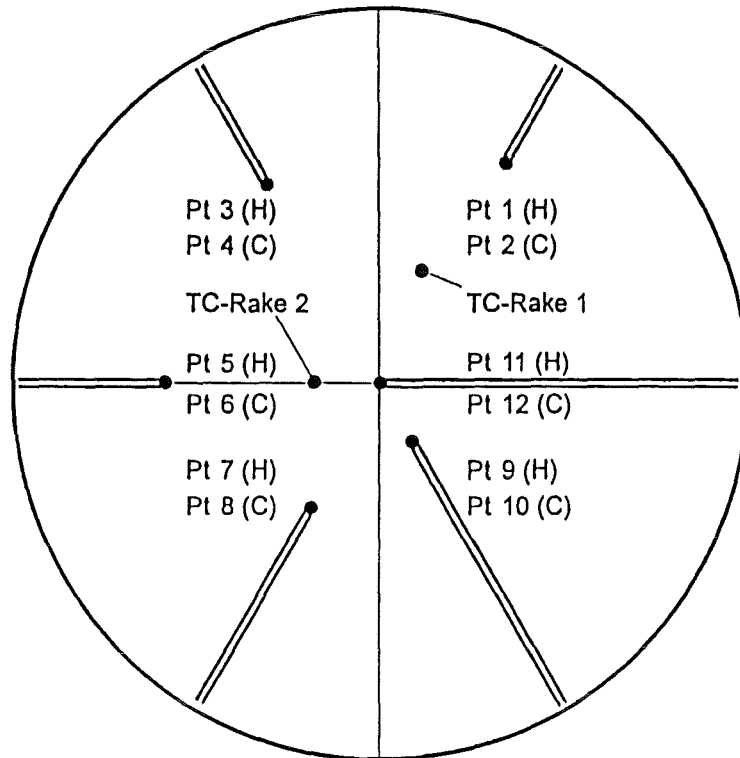


Fig. 2a: Radial positions of Pt-100 resistance thermometers in the heating (H) and cooling (C) plates and of thermocouple rakes TC-rake 1 and TC-rake 2 in the sodium layer, respectively

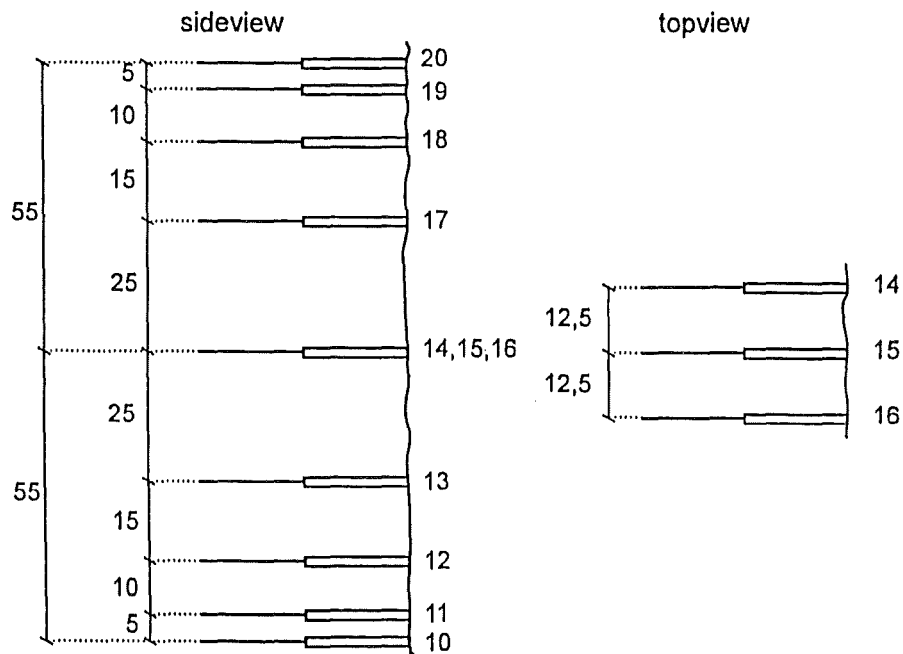


Fig. 2b: Axial positions of thermocouples on the TC-rake 2

$$Ra = \frac{\beta g h^3}{\kappa \cdot \nu} \Delta T_{sod}$$

$$\bar{a} = \frac{Q}{A} \frac{1}{6} \sum_{j=1}^6 \frac{1}{\Delta T_{sod}(j)} \quad (1)$$

$$Nu = \frac{\bar{a} h}{\lambda_{sod}}$$

Here  $\beta$  is the coefficient of thermal expansion,  $g$  the acceleration of gravity,  $h$  the layer height,  $\kappa$  the thermal diffusivity,  $\nu$  the kinematic viscosity,  $Q$  the total heating power,  $A$  the total heated sodium surface,  $\Delta T_{sod}$  the arithmetic mean temperature difference across the sodium layer and  $\lambda_{sod}$  the thermal conductivity of sodium.  $\Delta T_{sod}$  is evaluated from the difference between opposite pairs of resistance thermometers, allowing for the temperature differences inside the copper plates between the thermometers and the surface in contact with the sodium. The temperature differences are calculated assuming a constant mean heat flux at the heating plate.

Temperature time signals are recorded from the Pt-100 resistance thermometers and the thermocouples inside the copper plates and the thermocouples protruding into the sodium layer from the two rakes. Steel sheathed Ni-Cr-Ni thermocouples of tip diameter 0.25 mm were used. Their undamped frequency response is about 40 Hz (see Bremhorst et al (1989)). The signals are then evaluated for the RMS-value, the skewness  $S$  and flatness  $F$ . Additionally, auto- and cross-correlations  $\Phi$  and cross power density spectra are calculated. The definition and evaluation procedure for these functions can be found in any textbook on turbulence statistics e. g. Lumley (1970). The sampling frequency is varied from 1 to 20 Hz depending on the heating power and hence the observed time scale in the temperature signal, in order to resolve signal properties up to 10 Hz. The evaluation is performed with the aid of a commercial software package PlotIT (1990). Up to 10 000 points are generally taken for evaluating the statistical properties and then processed for the plots. For mean values, 150 points are usually taken with a sampling rate of 0.2 Hz which means an averaging time of 750 seconds.

## 4. Results

### 4.1 General observations

A striking observation during the performance of the experiments is the fact that the temperature fluctuations are well sensed from the turbulent sodium flow by the Pt-100 resistance thermometers located in the copper plates at a distance of 25 mm from the wetted surface. This is not surprising as the thermal conductivity of copper ( $\lambda_{Cu} \approx 380 \text{ W/mK}$ ) is only about 5 times larger than that of sodium ( $\lambda_{Na} \approx 75 \text{ W/mK}$ ). Moreover, the thermal diffusivities of copper and sodium are nearly equal. Thus, the experimental situation is far from the usual isothermal boundary condition<sup>1)</sup>. Fig. 3 shows a typical temperature history recorded by six Pt-100 thermometers in the heating plate for a heating power of 14 kW in a time interval of 1400 s. During this particular experiment all the sensors are placed in the bore holes at the same radial distance of 80 mm from the rim of the test section but separated azimuthally by a 60° subdivision. Clearly, the copper has a damping effect on the high frequency content of the original temperature fluctuations, but the low frequency structure of all six temperature traces show a

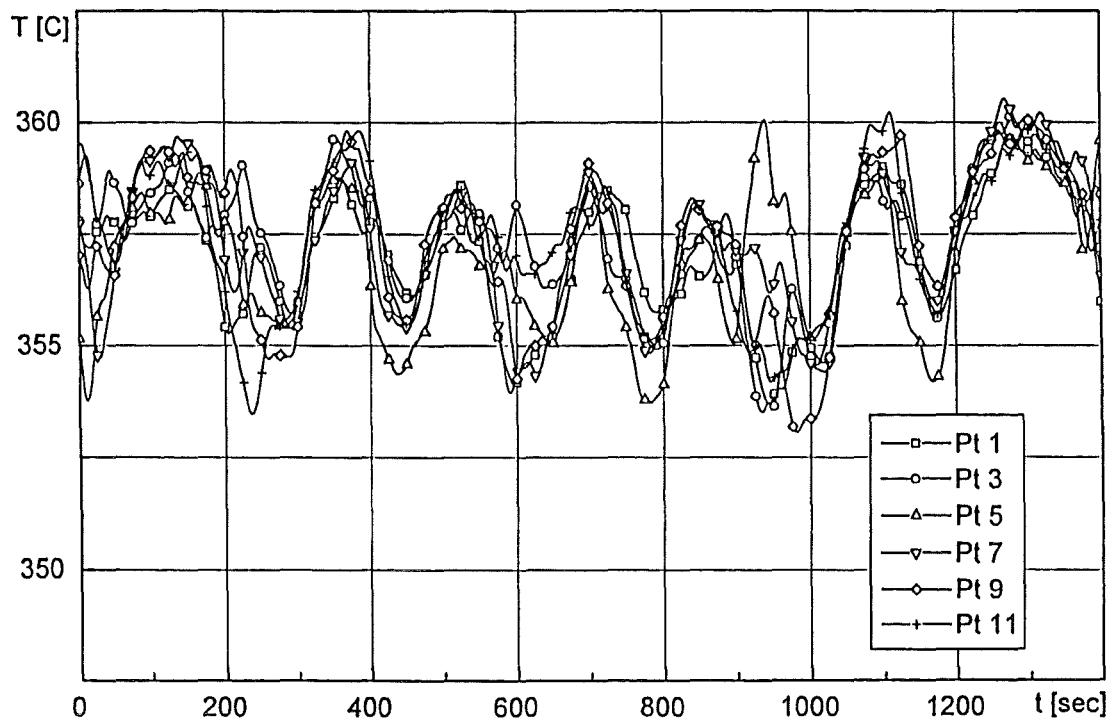


Fig. 3: Temperature histories of the six Pt-100 thermometers each separated by 60° on a radial position  $r/R = 0.7$ . Power supply is varied from 11 kW to 14 kW and down to 5 kW

1) The relevant Biot number  $Bi = \lambda_{Cu}/\lambda_{Na} \cdot h/d$  has a value of about 10

high coherency. Cross-correlations of the signals recorded by the different resistance thermometers result in correlation coefficients ranging between 0.69 and 0.86. The same observations have been made for other heating powers. The very low frequencies in fluctuating Bénard convection can be associated with a slow motion of cellular patterns. We infer from the coherency of the signals that the flow pattern in the sodium layer maintains a high degree of axisymmetry. This axisymmetric coherency and the relatively small aspect ratio of the test chamber suggest that the convection pattern consists of two fluctuating concentric ring rolls. This type of flow pattern has been observed in the past in cylindrical containers heated from below, if for example the convection is simultaneously forced by small radial temperature gradients in the top or bottom plates in the vicinity of the vertical side wall (see e. g. Koschmieder, Pallas (1974), Stork, Müller (1975), Steinberg et al. (1985) and Zhao et al. (1995)). A sketch of the conjectured pattern is given in Fig. 4.

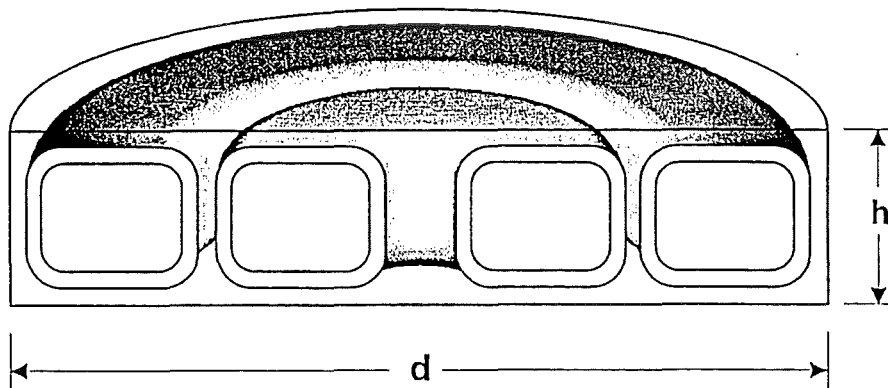


Fig. 4: Schematic sketch of the flow pattern for an aspect ratio  $d/h = 4.5$  of the sodium layer

The local mean surface temperatures (averaging time 750 s) can be seen in Fig. 5a as recorded by the Pt-100 thermometers in the cooling and heating plates at the tip of the bore holes (see Fig. 2a) for increasing heating powers. Moreover this graph shows the temperature variation at the copper plates in the radial direction. The temperature variations are generally larger for a given heating power at the cooling plate. The mean temperature difference across the layer is given in Fig. 5b as a function of the heating power. It is determined by averaging the temperature differences from all six pairs of resistance thermometers at an actual heating power. The graph shows that the heat transfer mode is subject to significant changes in the range between  $10 < \Delta T [K] < 15$ . This will have an impact on the Nusselt-Rayleigh number relation. The radial variation (compare Fig. 2a) of

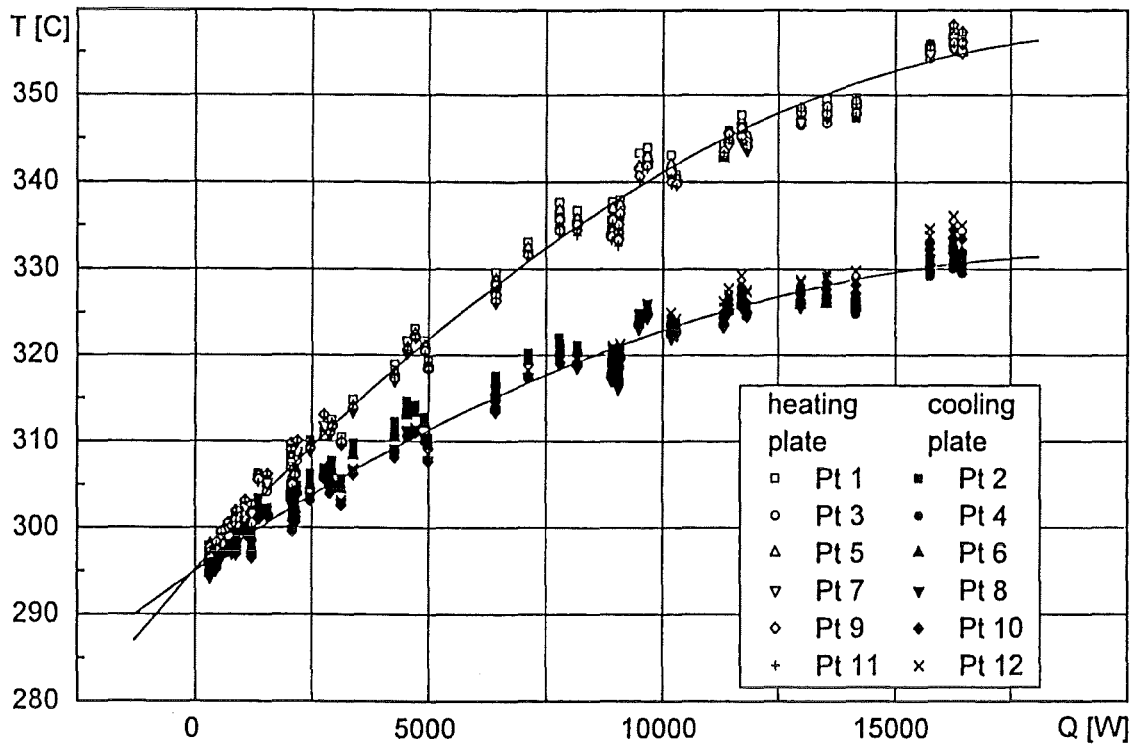


Fig. 5a: Measured local surface temperatures of heating and cooling plate

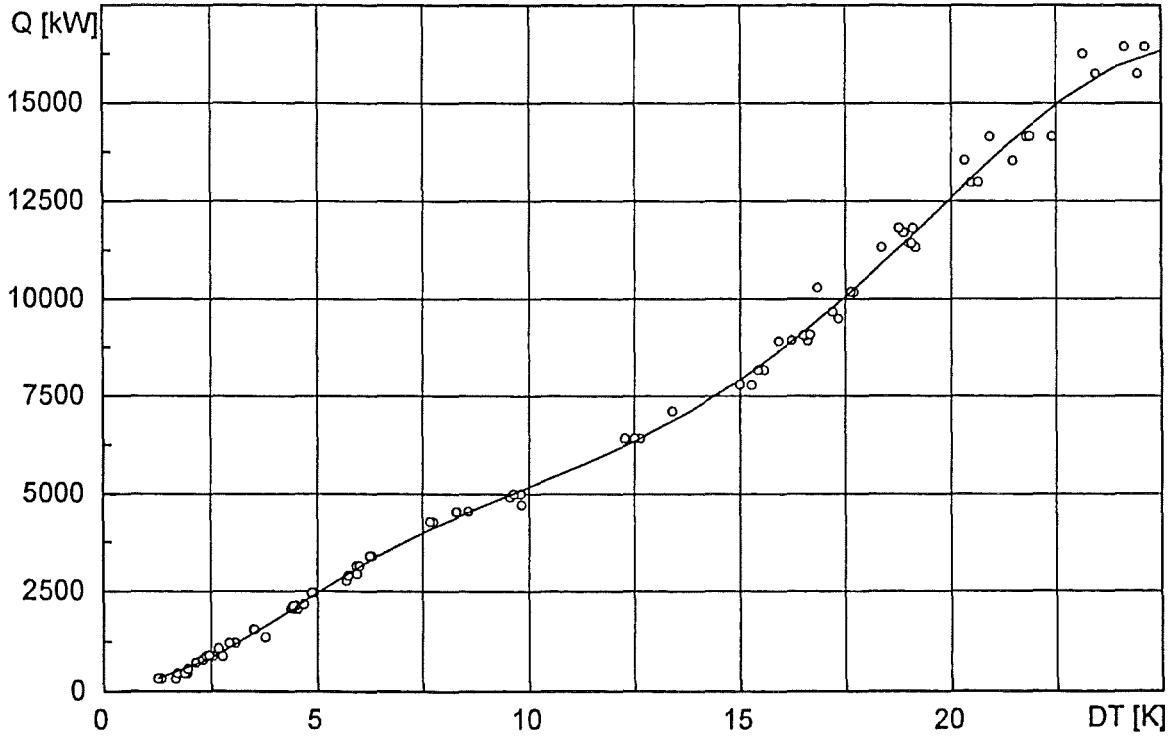


Fig. 5b: Measured mean temperature differences between the surfaces of heating and cooling plate versus heating power



the time averaged local temperature difference across the sodium layer and the associated Ra number can also be recognized in Fig. 6a for different power levels. The functional dependence of the fitting curves changes in the range  $7 \cdot 10^5 < Ra < 2 \cdot 10^6$  from a curve of mostly negative curvature to one with an inflection point and at  $Ra = 2.4 \cdot 10^6$  to a persistent positive slope. We suggest that this feature is associated with a transition between two different flow modes in the sodium layer. The non-uniformity of the temperature distribution measured in the heating and cooling copper plates indicates an intrinsic difficulty of heat transfer investigations in sodium layers. Since the heat conductivities of sodium and copper are of similar size (see above), ideal thermal boundary conditions such as constant temperature or constant heat flux conditions cannot be achieved. In particular, because of the convection flow pattern the temperature field in the sodium layer will have a feed back on the temperature distribution in the confining horizontal copper boundaries. This feed back mechanism is also reflected by the crossing of the two temperature difference curves shown in Fig. 6b. The particular temperature differences were measured at radial positions  $r/R = 0$  and  $0.7$ . Assuming an axisymmetric convection pattern as sketched in Fig. 4, the larger temperature difference  $\Delta T_6$  in the center compared to the smaller temperature difference  $\Delta T_1$  at the position  $r = 0.7R$  indicates a downflow in the center of the test chamber in the power range  $P \leq 6$  kW corresponding to  $Ra \leq 2 \cdot 10^6$  and an upflow for  $P \geq 8$  kW or  $Ra \geq 2.4 \cdot 10^6$ . The largest temperature differences are suggested to occur, where the temperature controlled cooling plate with finite conductivity has a cold spot. This is near a downflow region of the convection pattern. The heating plate behaves differently in the downflow area, since it is heatflux controlled and, as shown by the data of Fig. 5a, has a more uniform temperature distribution than the cooling plate.

#### 4.2 The dimensionless heat transfer $Nu(Ra)$

The dimensionless heat transfer graph  $Nu(Ra)$  can be evaluated using the data base of Figs. 5a and 5b and equation (1). The results are presented in Figs. 7a and 7b. The data plot in Fig. 7a indicates clearly two different heat transfer modes, one in a range  $Ra \leq 1 \cdot 10^6$  the other for  $Ra \geq 1.5 \cdot 10^6$  with a rapid decrease of the convective heat transfer inbetween. This drastic change in the  $Nu(Ra)$  graph is reflected in the slope changes of the heat transfer graph in Fig. 5b. The transition occurs at heating powers between 5 and 6 kW which correspond to Rayleigh numbers of  $1.2 \cdot 10^6$  and  $1.9 \cdot 10^6$ . We consider this "jump" in the Nusselt-Rayleigh number correlation another characteristic feature for a mode transition of the

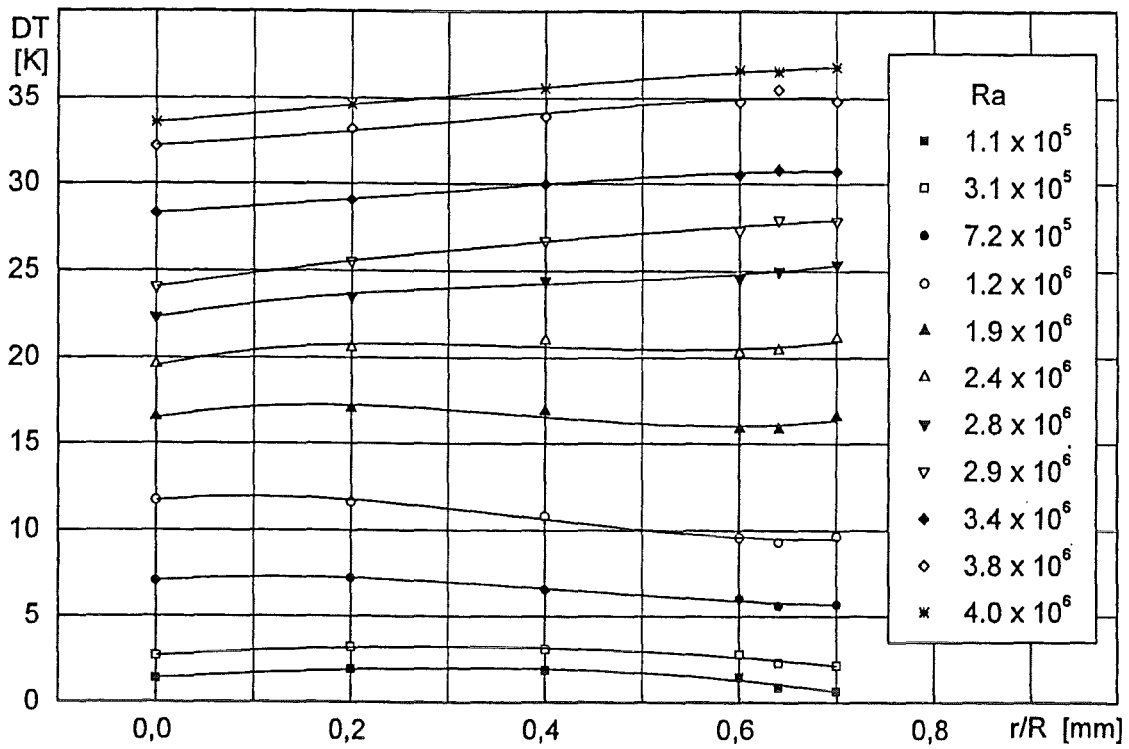


Fig 6a: Radial profiles of the mean temperature differences measured by the 6 pairs of opposite Pt-100 thermometers

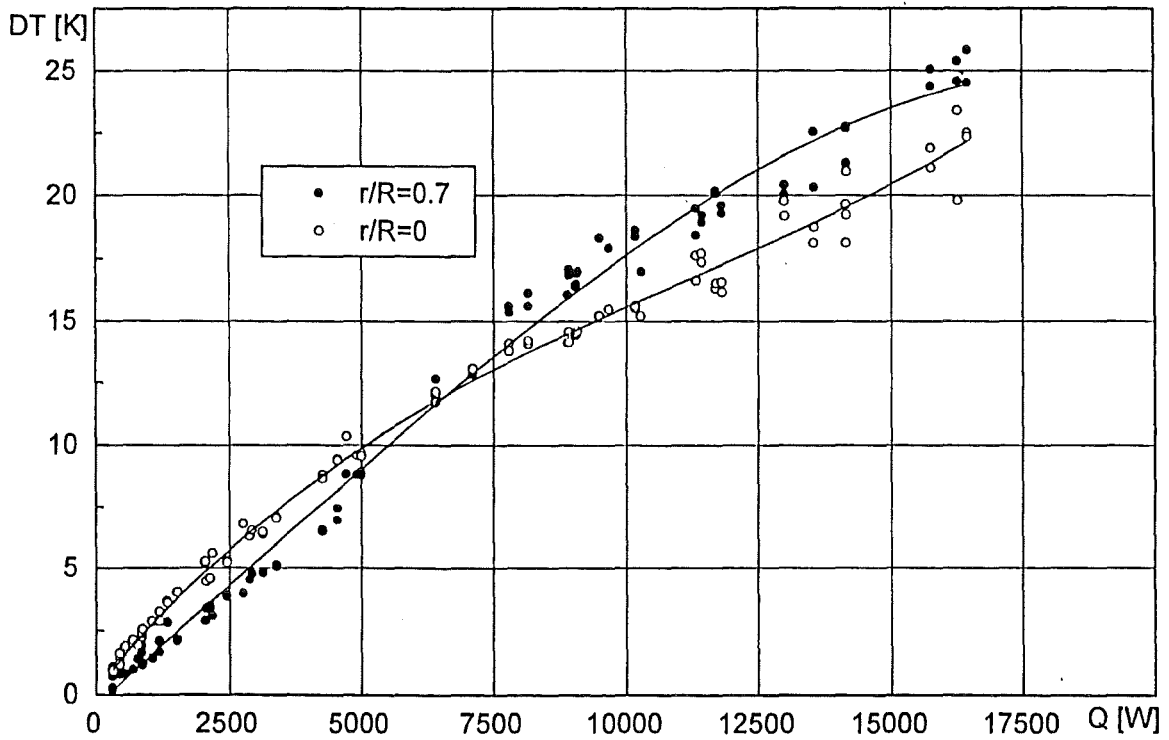


Fig. 6b: Mean temperature differences versus power supply at the positions  $r/R=0$  and  $r/R=0.7$ .

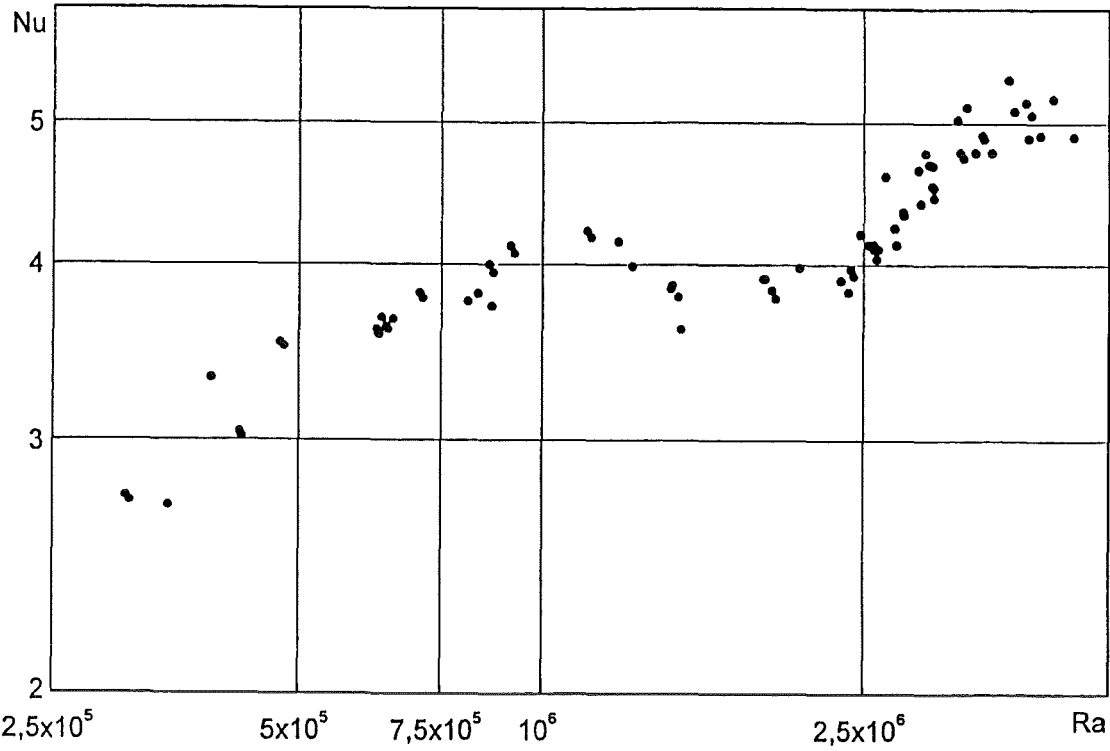


Fig. 7a: Dimensionless heat transfer correlation  $Nu(Ra)$  evaluated for the aspect ratio  $d/h=4.5$

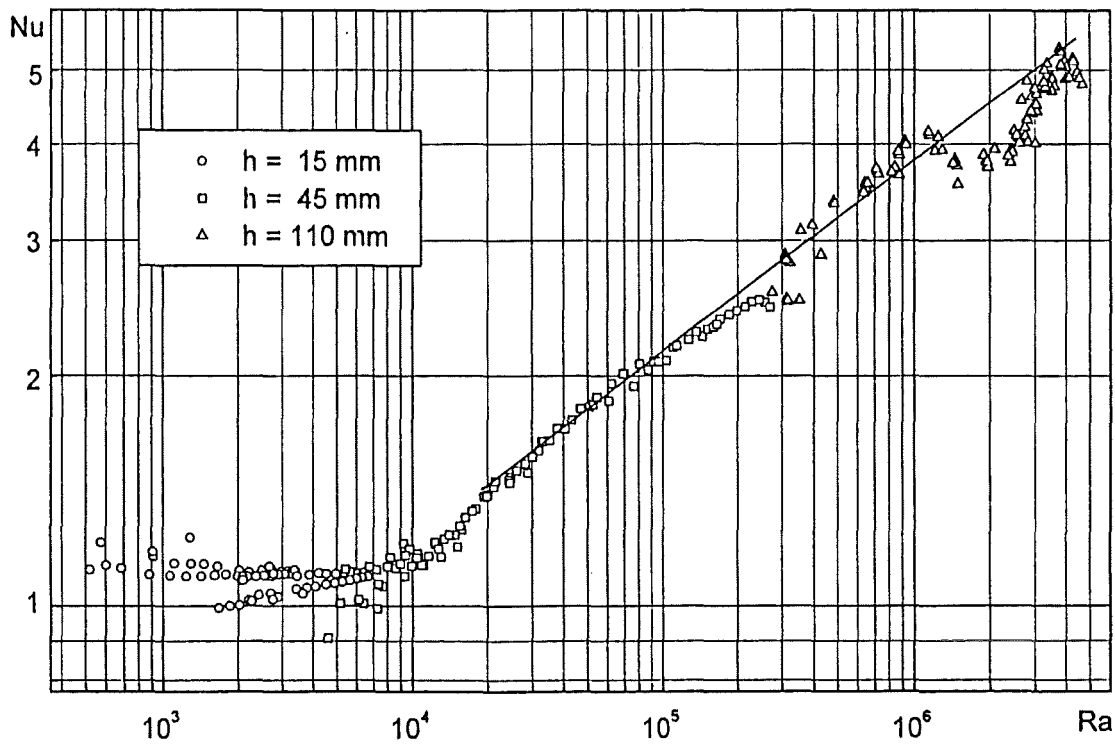


Fig. 7b: Dimensionless heat transfer correlation  $Nu(Ra)$  evaluated for the aspect ratios 33 (○○○), 11 (□□□) and 4.5 (△△△)

convection pattern which proceeds in a spatially and temporally fluctuating manner in this weakly turbulent flow regime. The transition zone corresponds to the change of shape in the radial temperature distribution of Fig. 6a and the crossover of the temperature differences in Fig. 6b. In Fig. 7b the new data are plotted together with heat transfer data for sodium obtained by Kek (1989) and Horanyi (1994) in containers of large aspect ratio  $d/h=33$  and 11 respectively. In the range  $2 \cdot 10^4 < Ra < 5 \cdot 10^6$  the data are well represented by the correlation

$$Nu = 0.115 Ra^{0.25} \quad (2)$$

If one considers  $10^6 < Ra < 3 \cdot 10^6$  as a range in which the heat flux is first perturbed by a change in the mode of convection in a test chamber of rather small aspect ratio  $d/h = 4.5$  but finally recovers, then the above correlation may be extrapolated also for the extended range of Rayleigh numbers up to  $Ra \leq 4.5 \cdot 10^6$ . Further experiments for even higher Rayleigh numbers are required to corroborate this conjecture.

#### 4.3 Axial mean temperature profiles in the sodium layer

Temperature distributions across the sodium layer, time averaged for 5000 seconds, are presented in Fig. 8. The profiles are obtained from the 9 thermocouples of rake probe 2 near the cell center. The most obvious feature in this graph is the formation of pronounced thermal boundary layers at the heating and cooling plates and a weakly decreasing temperature in the middle region of the layer for heating rates beyond 4 kW corresponding to  $Ra > 1.1 \cdot 10^6$ . The formation of the thermal boundary layers seems to correlate with the rapid change in the Nusselt Rayleigh number correlation of Fig. 7. The thickness of the boundary layer varies roughly between 10 and 20 mm. A crude evaluation of the boundary layer thickness by linear extrapolation of the temperature gradients at the wall and the center of the layer (see Fig. 8) indicates that the thermal boundary layer becomes unstable first at the heated bottom for  $Ra \approx 2.4 \cdot 10^6$ . Indeed, rough estimates of a Rayleigh number based on the evaluated thermal boundary layer thickness and the temperature drop across it at the bottom plate suggests that its value is significantly above  $Ra_\delta \approx 1100$ , which is the critical value for a heated horizontal layer with "free" upper surface. The onset of the boundary layer instability conforms with the drastic variation in the Nusselt number graph of Fig. 7. We conjecture that the instability of the thermal boundary layer triggers a change in the mode of convection. It is well known

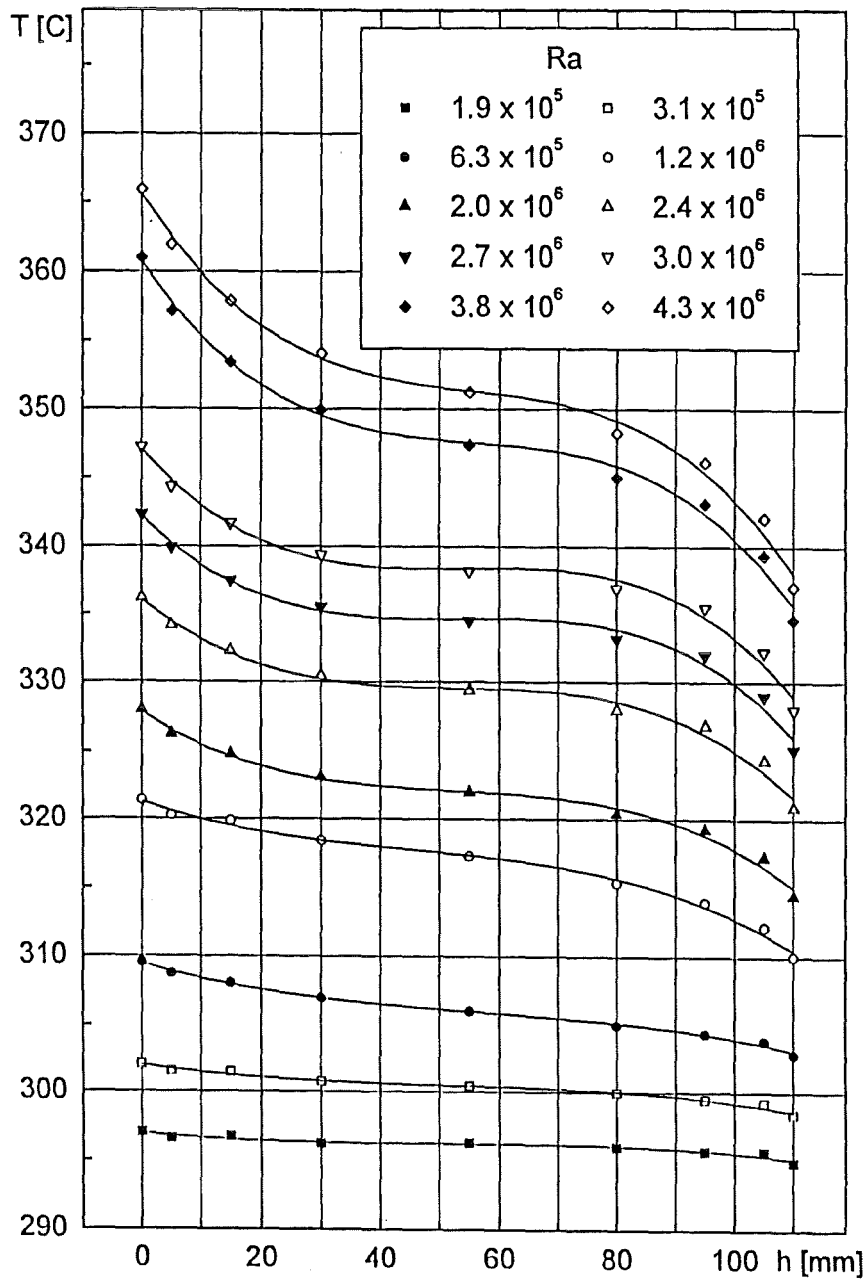


Fig. 8: Mean temperature profiles for different Ra-numbers across the sodium layer at the position of TC-rake 2

from convection experiments in containers with small aspect ratio (see Koster and Müller (1984)) that small perturbations such as instabilities of thermal boundary layers can trigger transitions between neighbouring convection modes of similar energy levels.

#### 4.4 Evaluation of temperature fluctuation signals

Temperature signals recorded by three thermocouples of the TC rake 2 probe (see Fig. 2a) are presented in Figs. 9a, b, c. The thermocouples are located at mid height of the layer ( $T_{15}$ ), in direct contact with the heated copper plate ( $T_{10}$ ) and in contact with the cooled copper plate ( $T_{20}$ ). The small scale, short term fluctuations with periods lower than 10 s exhibit the highest intensity at the layer mid height (see Fig. 9a). This is consistent with the idea, that the short term fluctuations are damped near the upper and lower boundaries. Otherwise Fig. 9a shows a long term uniform temporal behaviour. This long term character of the temperature signals changes drastically for the Rayleigh numbers  $Ra=2.8 \cdot 10^6$  and  $Ra=4.3 \cdot 10^6$  displayed in Fig. 9b and c. A new long period fluctuation of 300-400 s occurs which modulates the high frequency temperature fluctuations. Moreover, the intensities of the low frequency mode of modulation recorded by the three thermocouples are nearly equal. This observation suggests that the two

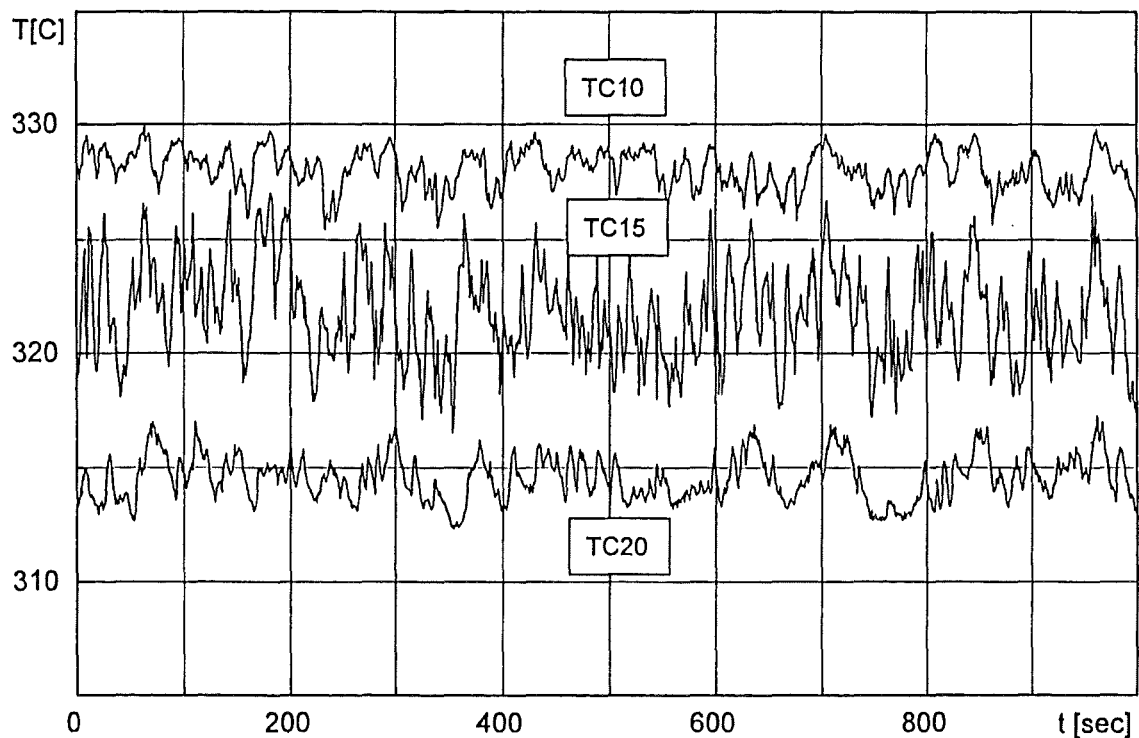


Fig. 9a:  $Ra=2 \cdot 10^6$

Fig. 9: Temperature histories recorded from thermocouples of TC-rake 2 at the axial positions: surface of heating plate (TC10), middle of sodium layer (TC15) and surface of cooling plate (TC20) for  $Ra=2 \cdot 10^6$  (a),  $Ra=2.9 \cdot 10^6$  (b) and  $Ra=4.3 \cdot 10^6$  (c)

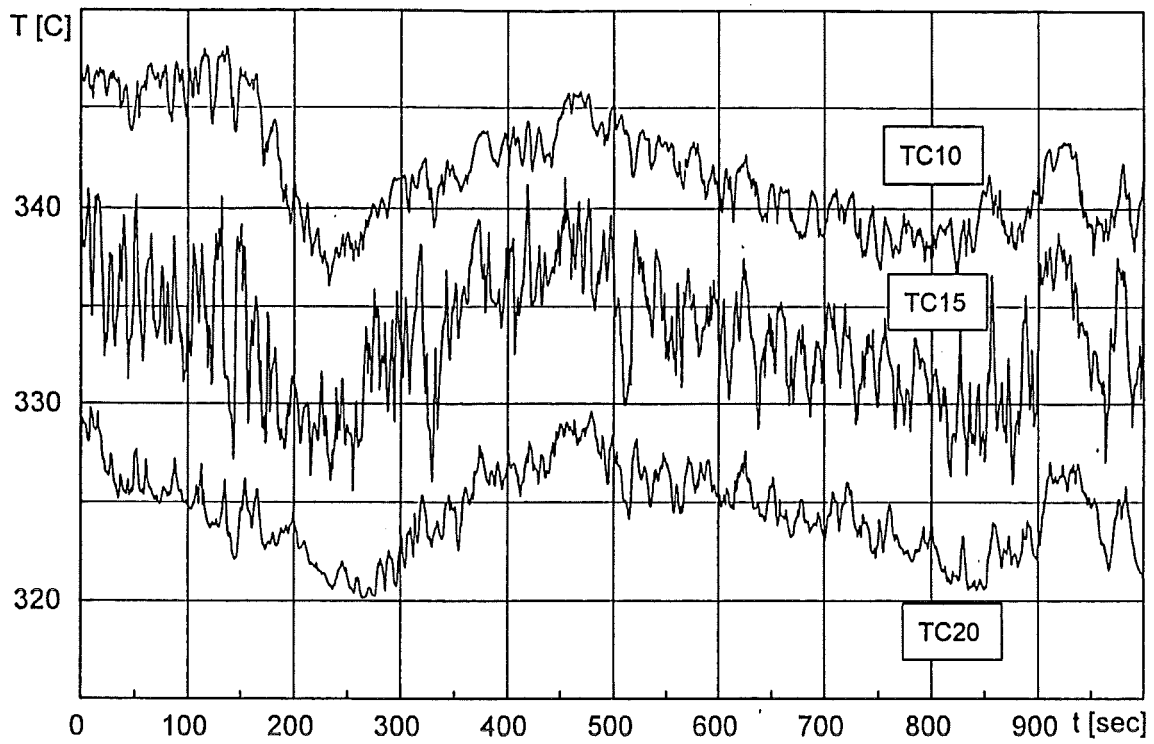


Fig. 9b:  $Ra = 2.9 \cdot 10^6$

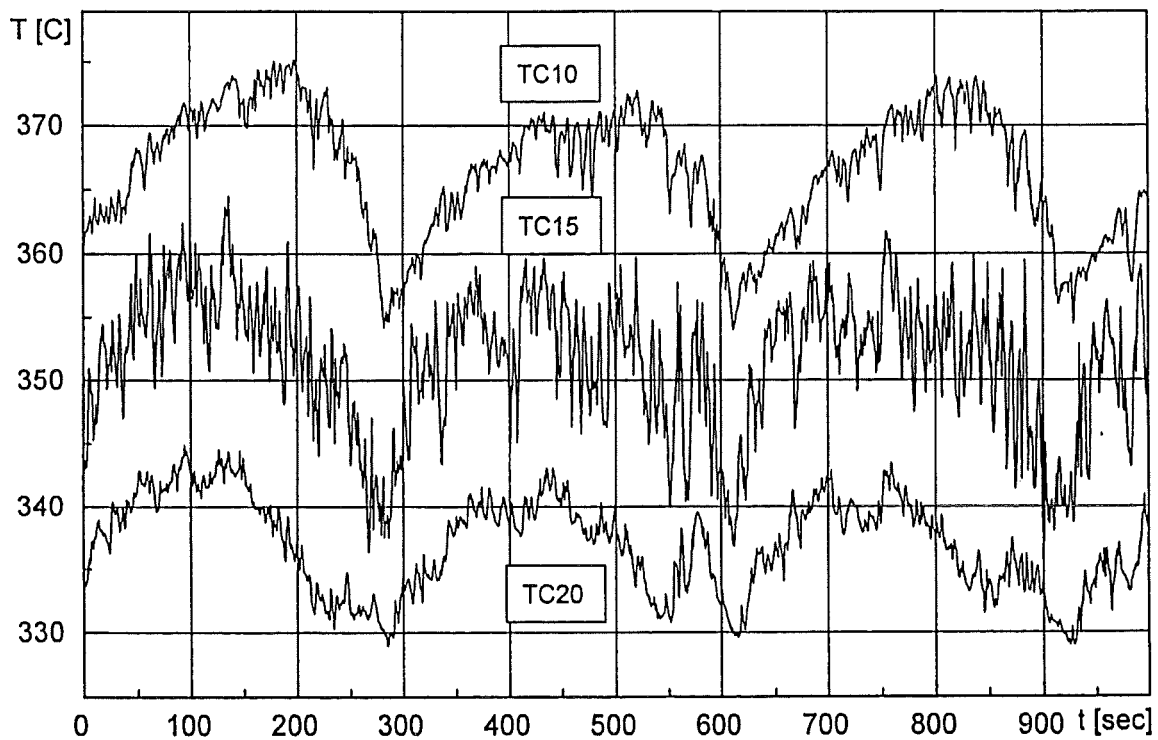


Fig. 9c:  $Ra = 4.3 \cdot 10^6$

different time scales of the temperature history may be associated with two relevant length scales of the experiment in this range of Rayleigh numbers, namely the thickness of the thermal boundary layer and the container dimensions related to the large scale wave length of the roll pattern. The small scale fluctuations in the order of a few seconds are consistent with the time for thermal diffusion across a thermal boundary layer of about 10-20 mm and a thermal diffusivity for sodium of  $7 \cdot 10^{-5} \text{ m}^2\text{s}^{-1}$  (see Fig. 8 and 11 for an assessment of the boundary layer thickness). The large scale fluctuation of the ring roll pattern can be imagined as a quasi periodic fluctuation of the free cell boundary located in a range near  $r/R \approx 0.5$  which is generally associated with a fluctuation of the intensity of the large scale convection velocity and thus generally correlates to the turn over time of an individual convection cell. But, we shall see below that in our case the turn over time of a few seconds is not compatible with the observed long period fluctuations.

The large scale temperature fluctuations are also sensed by the resistance thermometers in the copper plates. For the highest Rayleigh number  $Ra = 4.3 \cdot 10^6$  temperature signals are recorded by the thermometer at the center of the heating plate (PT6) and the one at the outermost position (PT1) at a distance of 80 mm from the rim. The temperature signals  $T_m$  are normalized by the mean

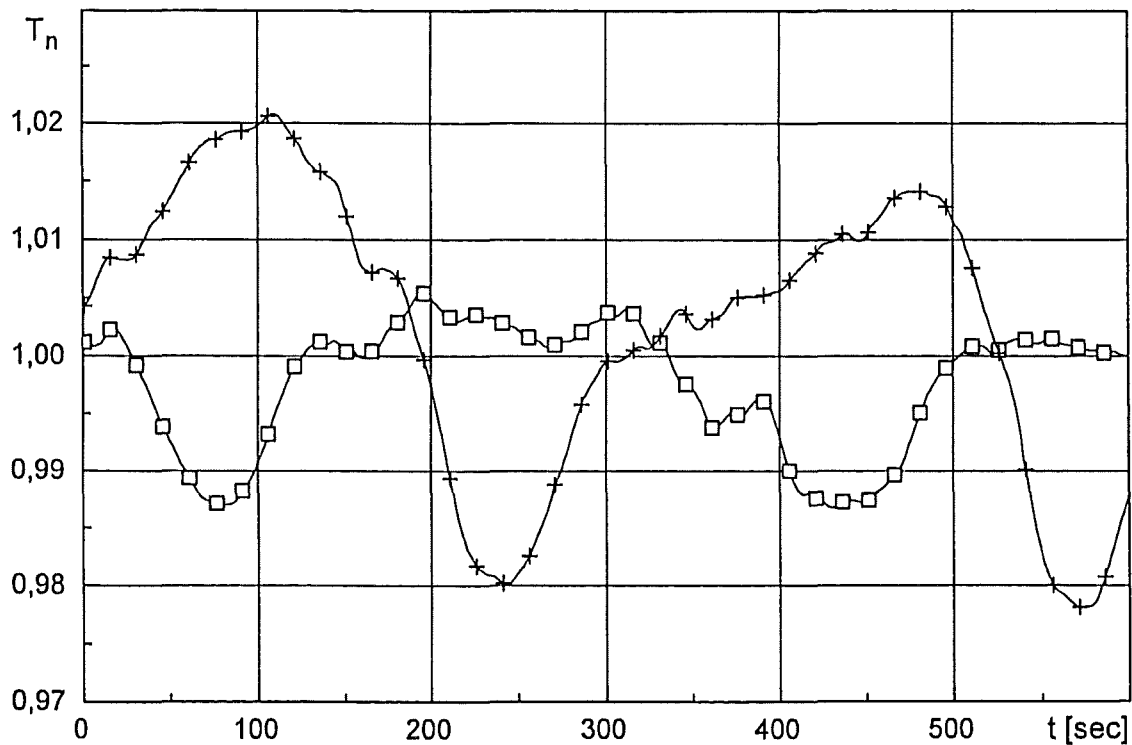


Fig. 10: Normalized temperature histories recorded from Pt-100 thermometers at the positions  $r/R=0$  (□ □ □),  $r/R=0.7$  (+ + +)



temperature averaged over 5000 s, and they are shown in Fig. 10. The two signals are nearly out of phase by 180°. Due to this phase shift of 200-300 seconds significant conductive heat fluxes occur within the heating plate. Taking one half of the horizontal extent of the test chamber as the relevant length scale for a conductive equalisation of the temperature and the thermal diffusivity of copper,  $\kappa_{\text{Cu}} = 1.2 \cdot 10^{-4} \text{ m}^2\text{s}^{-1}$ , we obtain a time scale of the order  $\tau \approx 100 \text{ s}$ . We conjecture therefore that the large scale temperature fluctuations are caused by an interaction of the convective heat transport in the sodium and the conductive equalization of temperature fluctuations in the bounding copper plates. The relaxation character of the long term temperature fluctuation recorded by the thermocouple  $T_{10}$  and shown in Fig. 9c is characteristic for a conduction-convection-controlled process. Relaxation oscillations in Bénard convection were first discussed by Busse (1967). Other possible origins of the long period oscillations such as fluctuations in the thickness of the thermal boundary layer or circulating hot spots can be excluded, since their time scales vary between 1.5 and 6 seconds.

The intensity of fluctuations, i. e. the temperature RMS value is a characteristic statistical property of a fluctuating temperature field. Fig. 11 shows the RMS values of the temperature distribution across the layer height measured by thermocouples at the rake 2 near the center of the test cell. The plotted values correspond to the mean temperature distributions shown in Fig. 8. The formation of a thermal boundary layer near the lower and upper boundaries of the container can be identified by the emergence of two maxima in the curves fitting the RMS values for Rayleigh numbers  $Ra \geq 1.2 \cdot 10^6$ . The unusual high level of the RMS values at the bounding copper plates underlines once more the fact, that the thermal boundary conditions are in general not ideal in sodium experiments, even, if copper is used as the material for the confining container walls. The normalized RMS values ( $RMS/\Delta T$ ) are plotted in Fig.12. These values are evaluated from the temperature signals of a thermocouple located at the mid height of the sodium layer. The graph displays the results from our recent measurements and also RMS values from previous investigations by Kek (1989) and Horanyi (1994). After a steep increase in the RMS value it levels off at between 10 and 20 % in the range  $3 \cdot 10^4 < Ra < 4 \cdot 10^6$ . We interpret the lower level of the RMS values in the range  $2 \cdot 10^5 < Ra < 5 \cdot 10^6$  as an indication of the difference in the flow patterns occurring in two different test sections with layer heights of 25 mm (Kek (1989), Horanyi (1993)) and 110 mm (new measurements).

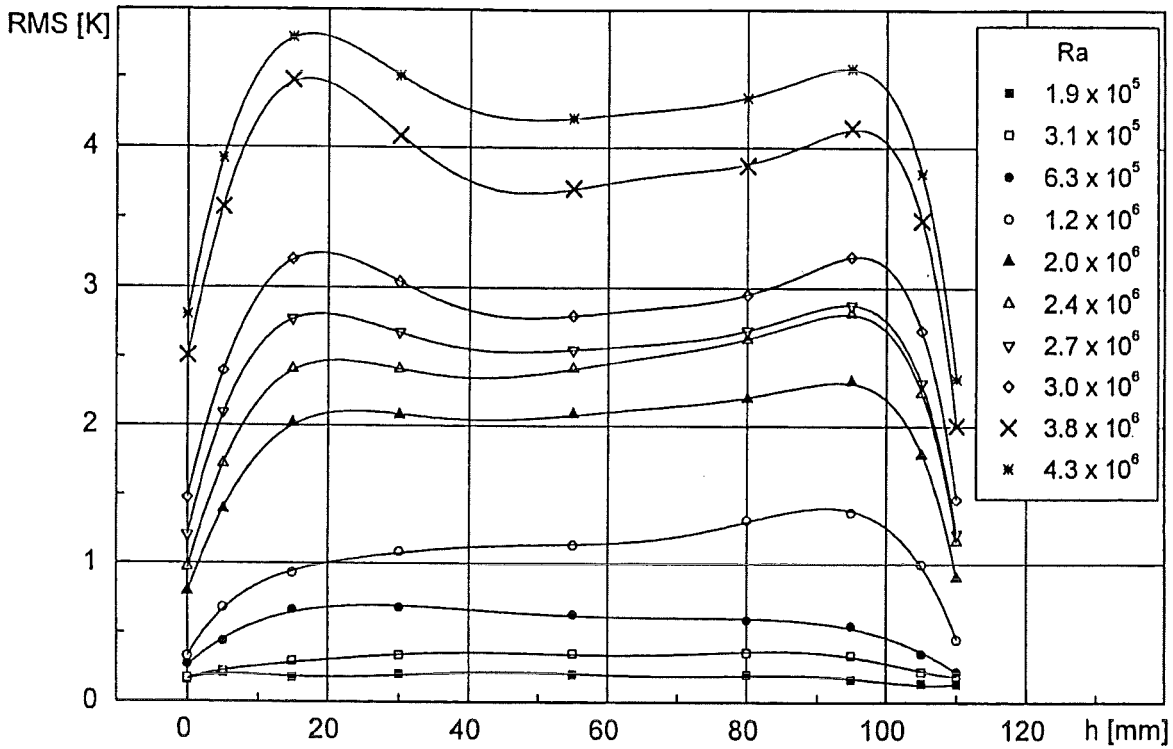


Fig. 11: RMS-profiles of thermocouple signals of TC-rake 2 across the sodium layer for different Rayleigh numbers

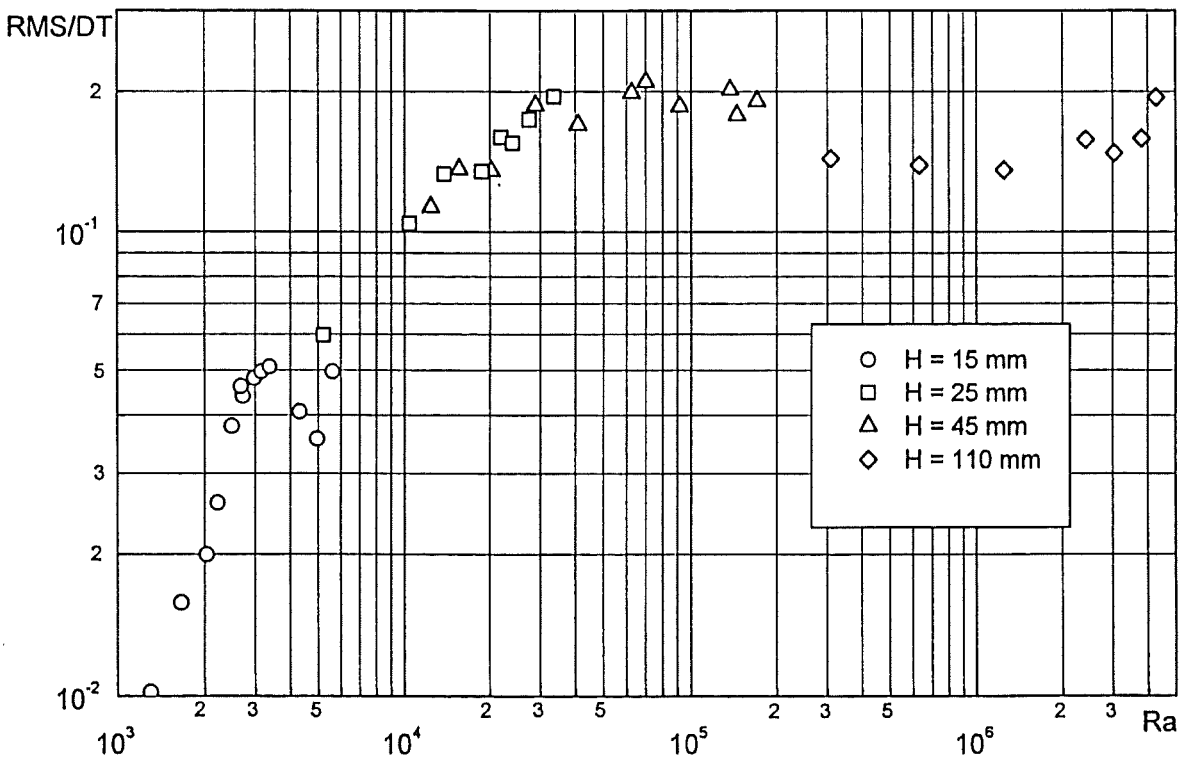


Fig. 12: RMS-values normalized by the mean temperature differences across the sodium layer versus Rayleigh number

Fig. 13 shows normalized power spectrum density functions (PSD) of the temperature signals  $E_T$  which are recorded in the center of the test chamber. The PSD functions are plotted for three different Rayleigh numbers,  $Ra = 3.55 \cdot 10^5$ ,  $1.45 \cdot 10^6$  and  $4 \cdot 10^6$ . It is seen that the cut-off-frequencies are generally lower than 1.2 Hz but increase with increasing Rayleigh numbers in the range from  $8 \cdot 10^{-2}$  to  $1.2 \cdot 10^{-1}$  Hz. All the three spectra decay with nearly the same power of  $E_T \sim f^{-4}$ . This latter finding is not consistent with the prediction of the spectral model of Batchelor et al. (1959) which gives a behaviour of  $E_T \sim f^{-17/3}$  for low Prandtl number fluids in the inertial-diffusive sub-range of the thermal energy spectrum. This subrange is specified by the Kolmogoroff and Batchelor time scales  $\tau_k = (\nu/\varepsilon)^{1/2}$  and  $\tau_b = (\kappa/\varepsilon)^{1/2}$ , where  $\nu$  is the kinematic viscosity,  $\kappa$  the thermal diffusivity and  $\varepsilon$  the viscous dissipation.

Using a refined similarity hypothesis by introducing a local length scale based on the strain rate, Gibson (1968) derived a spectral relationship  $E_T \sim f^{-3}$  in the limit of vanishing Prandtl number,  $Pr \rightarrow 0$ , in a frequency range

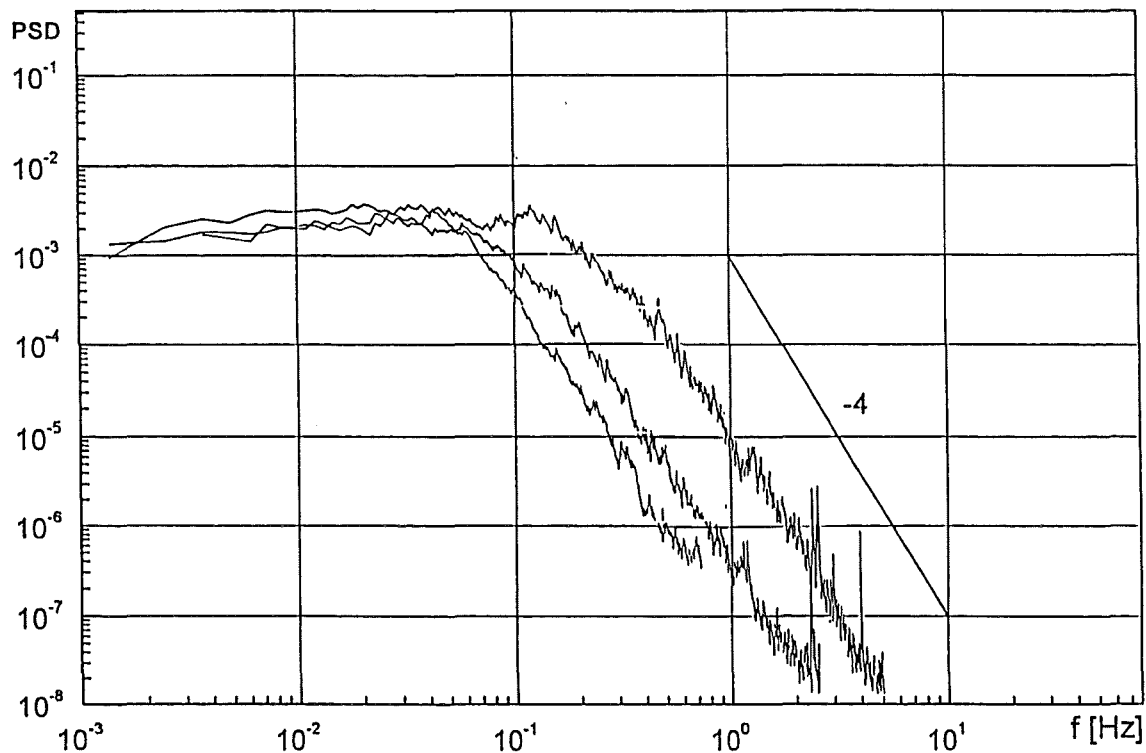


Fig. 13: Normalized power spectrum density functions of TC15 signals for the Rayleigh numbers  $Ra = 4 \cdot 10^6$  (A),  $Ra = 1.5 \cdot 10^6$  (B) and  $Ra = 3.6 \cdot 10^5$  (C)

$$2\pi \cdot v_b \left( \frac{\varepsilon}{\kappa^3} \right)^{1/4} < f < 2\pi \cdot v_b \left( \frac{\varepsilon}{\kappa^3} \right)^{1/4} \cdot Pr^{-1/4}.$$

In terms of integral parameters  $v_b = \left( \frac{Ra}{Pr} \right)^{1/2} \frac{\nu}{h}$

holds.2) For  $Ra=4 \cdot 10^6$  we get  $v_b=11.3 \text{ cms}^{-1}$ . Since Gibson's findings for the power decay apply for the limiting case  $Pr \rightarrow 0$  and a range of considerable higher frequencies, namely for  $1.7 \text{ s}^{-1} < f < 40 \text{ s}^{-1}$ , our stronger observed decay relation  $E_T \sim f^{-4}$  is unlikely to be due to an interference between the inertial range of the velocity spectrum and the diffusive range of the temperature spectrum. We suggest that the temperature decay occurs predominantly by molecular diffusion in a frequency range, where the first generation of energy containing eddies is generated by buoyancy release and where vortex generation by energy transfer to smaller size eddies is still negligible. Moreover, for the range of Reynolds number  $3000 < Re < 30000$  achieved experimentally the velocity PSD-function may not contain a marked inertial range at all. According to Tennekes and Lumley (1974) an inertial subrange exists only for  $Re > 10^5$ . The Reynolds number is here defined as  $Re \doteq (Ra/Pr)^{1/2}$ .

In his book Hinze (1979, p. 283) outlines for the case of small Prandtl number fluids that the power spectrum density (PSD) of a passive scalar, here the temperature, should scale as  $E_T(f, t) = H \kappa^{-3} E(f, t) \cdot f^{-4}$  in a turbulent velocity field. Here  $E(f, t)$  is the PSD of the velocity field. In the frequency range of the power containing eddies  $E(f, t)$  can be assumed constant. Thus the temperature power spectrum is purely diffusive under these conditions and has a  $E_T \sim f^{-4}$  dependency. This seems to be consistent with our observations.3)

Up to now there exist no direct measurements of the velocity in high Reynolds number liquid metal flow which allow a thorough analysis of the velocity time series. Such measurements are highly desirable to clarify the uncertainties concerning the spectral models for low Prandtl number turbulent flows.

---

2) The discussions of Batchelor et al. (1959) and Gibson (1968) are originally given in the wave number space. In this paper their results are transformed by Taylor's hypothesis to the frequency space. The equivalence of the normalized wave number and frequency spectra has been demonstrated by Chilla et al. (1993).

3) It is obvious, that the measured spectra do not contain a buoyancy range of influence according to Bolgiano (1959) with a behaviour of  $\varepsilon_T \sim k^{-7/5}$  as discussed by Cioni et al. (1996).

In order to assess the magnitude of the vertical velocity in the sodium layer, cross-correlations were performed between the signals of thermocouples TC 13 and TC 17 of rake 2 (see Fig. 2a). The velocities evaluated from the temperature fluctuations are shown as a function of the heating power in Fig. 14. For Rayleigh numbers  $Ra < 1 \cdot 10^6$  we find a velocity in downward direction in the center of the test chamber; for  $Ra \geq 2 \cdot 10^6$  the flow direction is upward. This finding corroborates our previous conjecture obtained from discussions of Figs. 5 and 6, namely that a change of the flow pattern occurs in the power range  $4000 < Q < 6000$  W, i. e.  $1.2 \cdot 10^6 < Ra < 2 \cdot 10^6$ . The measured velocities vary between a few mm/s and 100 mm/s. This is consistent with an evaluation of the buoyant velocity  $v_b$  obtained from the measured Rayleigh number at corresponding heating powers. We obtain, for instance, a velocity of  $v_b = 11.3 \text{ cms}^{-1}$  for  $Ra = 4 \cdot 10^6$ . This corresponds to the measured velocity of  $v_s \approx 13 \text{ cms}^{-1}$ . There is a reasonable agreement in the order of magnitude, if one takes into account the uncertainties which exist for the temperature correlation measuring technique in sodium with its large thermal diffusivity (see Mika (1975) and Koppermann (1983)). In spite of the quantitative uncertainties in cross correlation measurements for low fluid velocities in liquid metals, the change from negative to positive velocities is obvious.

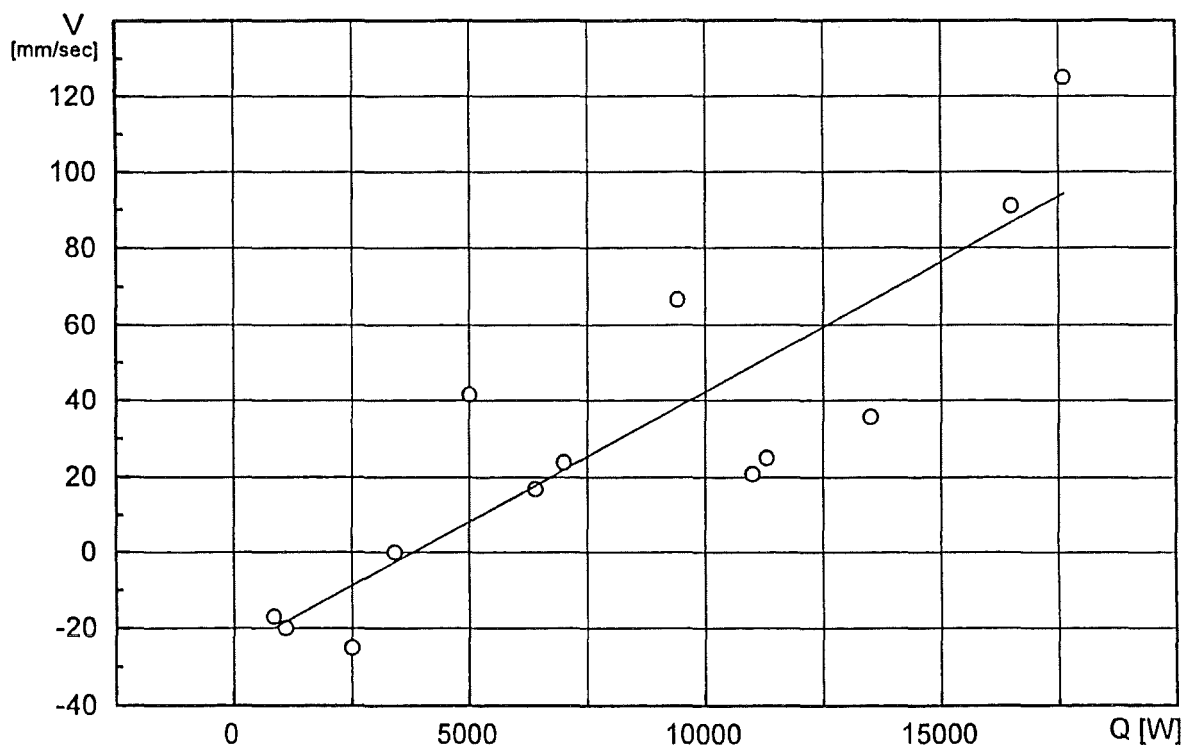


Fig. 14: Signal velocity of temperature fluctuations obtained from cross-correlation of temperature signals of TC 13 and TC 17

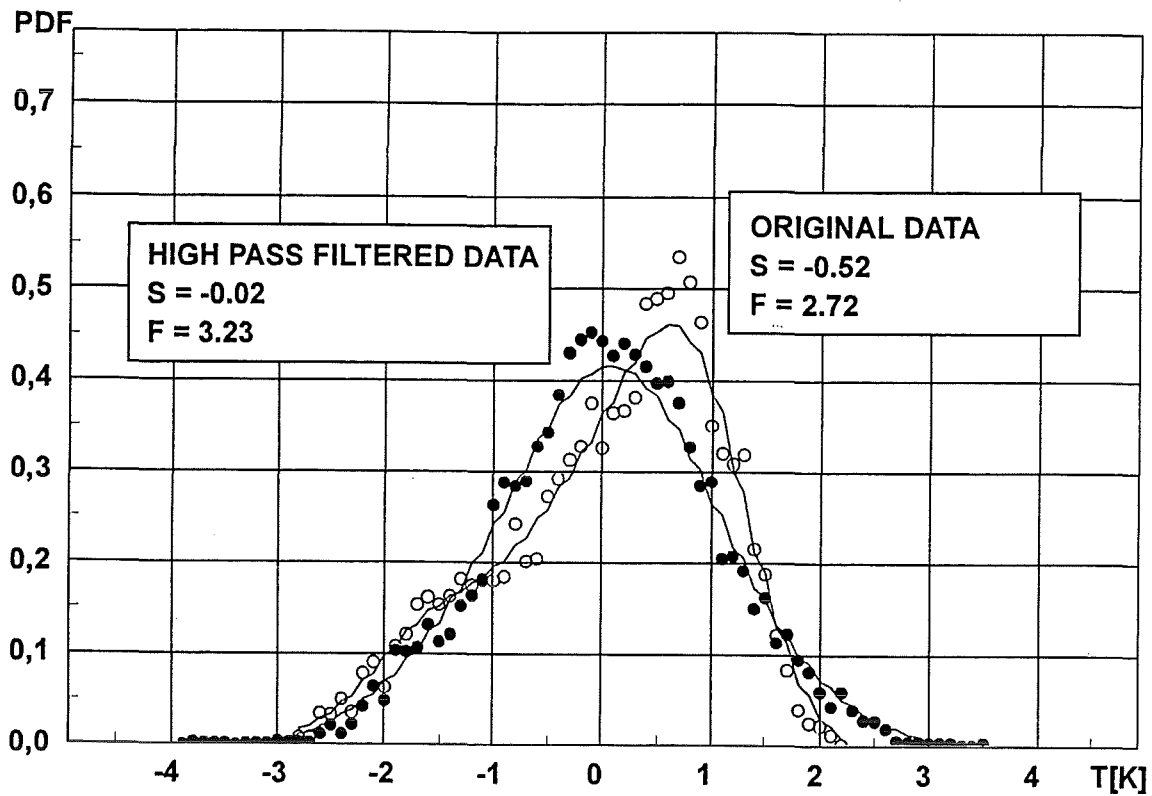


Fig. 15a: TC 15

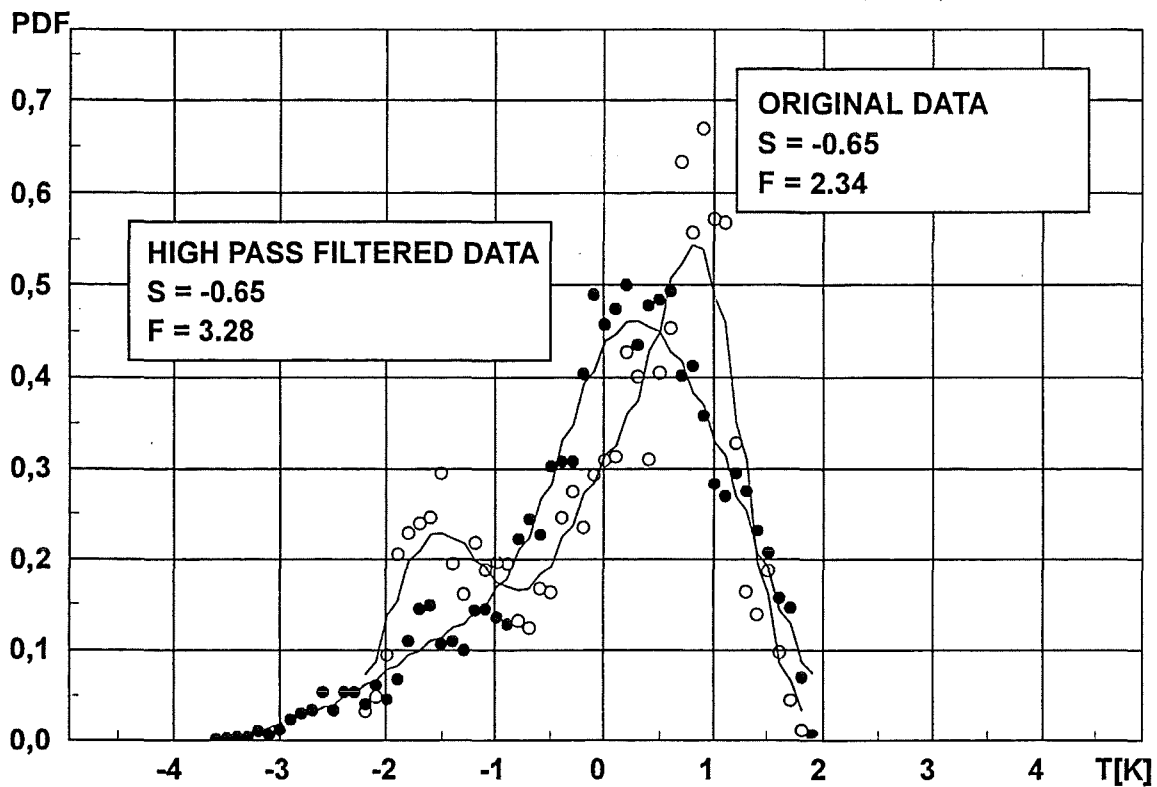


Fig. 15b: TC 10

Fig. 15: Normalized probability density functions of temperature signals of TC 15 (a) and TC 10 (b) for  $Ra = 4 \cdot 10^6$ . Comparison of original (○) and high pass filtered (●) data

The quality of turbulent flow has frequently been assessed from the character of the probability distribution function (PDF) of fluctuating signals, as for instance of temperature time signals (see e. g. Heslot et al., 1987). Figs. 15a, b and Fig. 16 show normalized PDFs for Rayleigh numbers  $Ra=3.5 \cdot 10^5$ ,  $1.45 \cdot 10^6$ ,  $4 \cdot 10^6$ . The PDFs were evaluated from temperature signals recorded by the thermocouple TC 15 of rake 2 in the middle of the sodium layer and thermocouple TC 10 on the surface of the heating plate.

For a high Rayleigh number  $Ra=4 \cdot 10^6$  the PDF of the unfiltered temperature signal TC 15 results in a skewed distribution. This can be seen in Fig. 15a. When the low frequency content of the temperature signal is filtered by a high pass filter with a cut-off-frequency of  $2 \cdot 10^{-2}$  the PDF becomes a nearly Gaussian distribution with a very low skewness,  $S=0.02$ , and a flatness of  $F=3.2$ . This indicates that a uniform small scale fluctuation "rides" on a long term, large scale motion. The Gauss like distribution of the filtered signal suggests, that a quite regularly structured, weakly turbulent convection exists for Rayleigh numbers of the order  $10^6$  which Castaing et al. (1989) term "soft turbulence". It is obvious from the filtering process, that the skewness  $S=-0.52$  of the unfiltered signal originates from the oscillatory, low frequency content of the temperature signal. For the same reason the flatness value decays below  $F < 3$ . Compared with the higher frequency parts of the signal the large scale fluctuating motion becomes even more evident, when the temperature time signal is evaluated for thermocouples at the heating or cooling plate. The PDF function is presented in Fig. 15b for a temperature signal at the cooling plate (see Fig. 9c, TC 10). The unfiltered signal shows two clear peaks, the smaller one reflecting the quasi periodic long term oscillation of the overall signal. Both, the filtered and the unfiltered signal have a skewness of  $S=-0.65$  but they differ by the flatness which becomes  $F=3.3$  for the filtered signal and  $F=2.3$  for the unfiltered signal.  $F=3.3$  still reflects the Gaussian similarity of the small scale fluctuations but because of the proximity of the hot wall some intensive cold spikes within a rising mean flow result in a significant skewness of  $S=-0.65$ .

The PDF's for Rayleigh numbers  $Ra=3.5 \cdot 10^5$ ,  $Ra=1.45 \cdot 10^6$  (signals recorded from the thermocouple TC 15 in the middle of the sodium layer) are shown in Fig. 16 and 17. They exhibit a significant asymmetry with skewness of opposite sign ( $S=0.47$  and  $S=-0.47$ , respectively). The change of sign in the skewness is another indication of the change of the overall mode of convection from down flow to up flow in the center of the test chamber. In general, there is an obvious trend in the

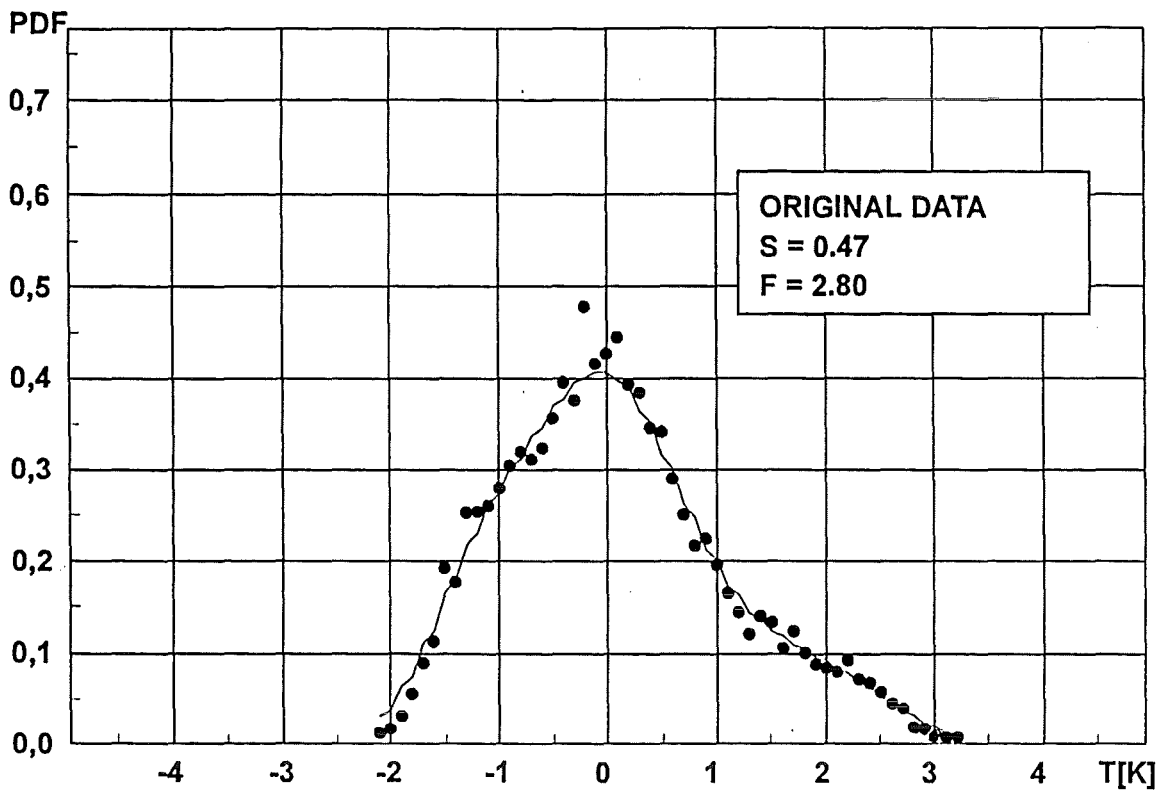


Fig. 16: Normalized probability density function of temperature signal of TC 15 (original data) for  $Ra = 3.6 \cdot 10^5$

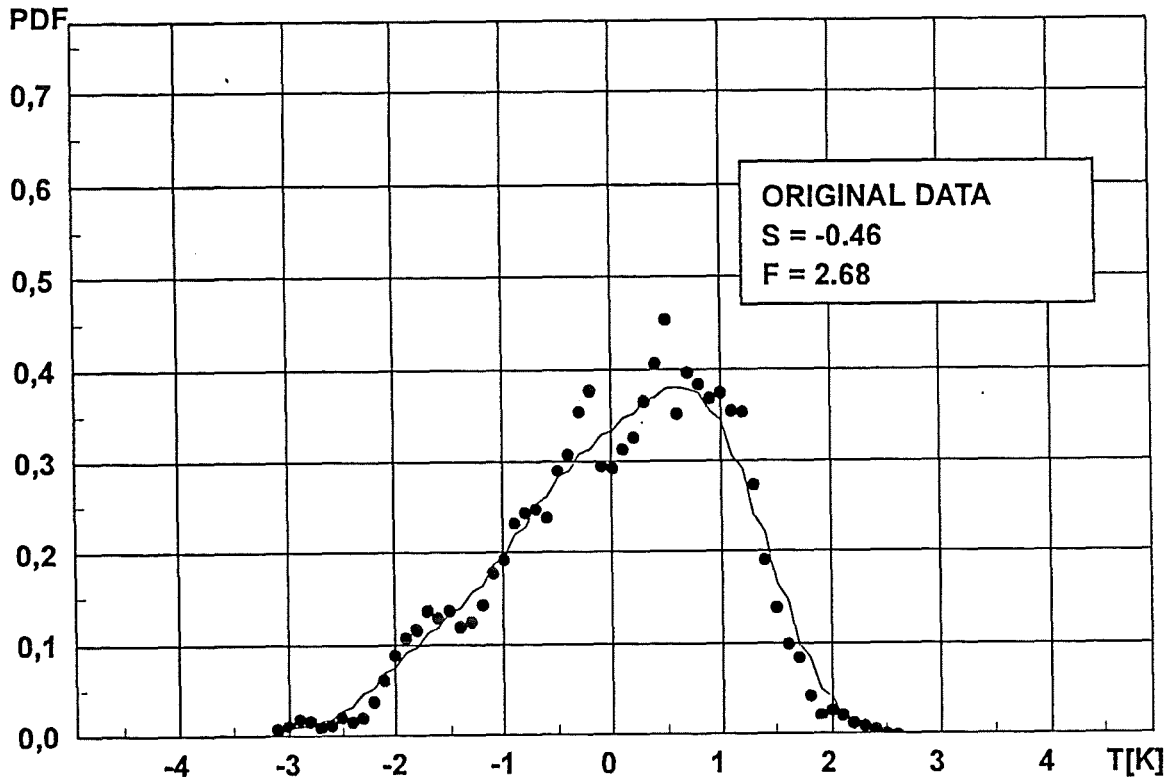


Fig. 17: Normalized probability density function of temperature signal of TC 15 (original data) for  $Ra = 1.5 \cdot 10^6$



small scale fluctuations from an asymmetric distribution towards a symmetric quasi Gaussian distribution in the bulk flow with increasing power level i. e. increasing Rayleigh numbers. More skewed distributions are observed near the outer edge of the thermal boundary layer. This can be seen in Fig. 18a, which shows the distribution of skewness across the layer height at the position of the thermocouple rake 2. The corresponding flatness distribution for the same conditions are given in Fig. 18b. The values at Rayleigh number  $Ra > 10^6$  seem to center around  $F \approx 2.5$ ; this value is noticeably smaller than  $F=3$  for the Gaussian distribution. This indicates, that the temperature signal in the center of the test chamber has become voided of short pulsed temperature spikes whereas the slow oscillatory content of the temperature signals remain undamped. This is reasonable as temperature disturbances generated in the boundary layers lose their identity by thermal dissipation along their path of transportation.

## 5. Discussion and Conclusions

Our recent sodium experiment in a cylindrical test chamber of aspect ratio 4.5 is characterised by an axisymmetric large scale convection in form of two concentric

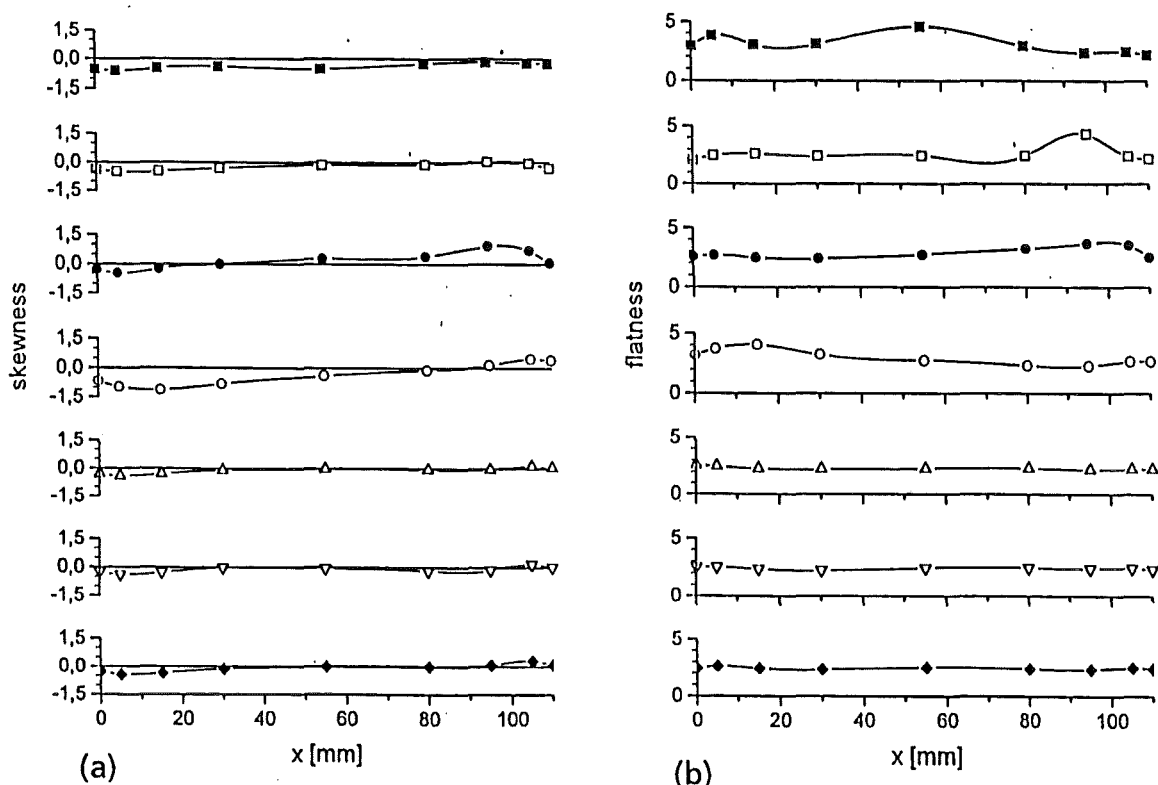


Fig. 18: Profiles of skewness (a) and flatness (b) for different Ra-numbers across the sodium layer at the position of TC-rake 2

ring cells (see Fig. 4). For low Rayleigh numbers  $Ra < 10^5$  there is a down flow in the center of the test chamber. A transition to a velocity field with up flow in the center occurs in a Rayleigh number range  $1 \cdot 10^6 < Ra < 2 \cdot 10^6$ . A thermal boundary layer forms at the heating and cooling plate simultaneously with this transition. An evaluation of the local Rayleigh numbers in the thermal boundary indicates that the thermal boundary layers become unstable at an overall Rayleigh number  $Ra > 2.4 \cdot 10^6$ , first at the heating plate and at higher values  $Ra$  also at the cooling plate. These thermal instabilities seem to trigger a large scale, long term relaxation oscillation of the overall convective flow, which we interpret as a conduction controlled process governed by the comparable heat conductivities of the test fluid sodium and the confining copper boundaries.

The observed temperature fluctuations in a Rayleigh number range  $Ra < 10^6$  without pronounced temperature boundary layers are mainly controlled by the convection of the velocity field and the thermal diffusion of slight local temperature inhomogeneities. The temperature behaves as a passive scalar. This passive behaviour of the temperature field is confirmed by the strong spectral decay of the temperature fluctuations with a power law  $E_T \sim f^{-4}$  as demonstrated in Fig. 13. The passive character of the temperature field is continued even into the thermally unstable range of the temperature boundary layers up to Rayleigh number  $Ra \sim 5 \cdot 10^6$ . As the turn around time for the large scale velocity field at high Rayleigh numbers  $Ra > 10^6$  is smaller or, at most, of the same order as the formation of thermal instabilities of the temperature boundary layer, the temperature inhomogeneities are quickly carried along with the fluid flow, wherein they lose their identity by thermal dissipation. There is no indication of an interaction between the velocity fluctuation field and the temperature fluctuation field; nor is there any signature of a direct influence of the gravity field on thermal inhomogeneities. This is clearly recognized from the absence of inertia or buoyancy influenced subranges with  $E_T \sim f^{-5/3}$  and  $E_T \sim f^{-7/5}$  respectively in the power density spectra of the temperature in Fig. 13. This is not surprising as the actual velocities in the test chamber result only in Reynolds numbers  $Re < 30000$ . These values are too low to generate inertial effects in the spectral decay of the kinetic energy of eddies generated by hydrodynamic instabilities (see Tennekes, Lumley (1974)). The energy in the velocity field is therefore mainly tied to the large scale, buoyancy induced roll vortices and to relatively well ordered low mode fluid dynamic instabilities of related shear flows in the wall regions or to the local oscillations of unstable detaching flows near the free vertical boundaries of the convection cells. One also has to keep in mind the wave

like instabilities along the convection rolls in low Prandtl-number flows described by Busse (1972). These relatively soft fluctuations of the velocity field are reflected in the nearly Gaussian character of the probability density functions observed in our experiments for the temperature histories recorded in the whole range of Rayleigh numbers achieved. Castaing et al. (1989) introduced the notation "soft turbulence" for this type of fluctuating flow governed by a relatively small number of instability modes, which in the case of a closed flow are likely to be characterized by a finite number of discrete wave lengths giving rise to chaotic interactions.

If one accepts - as suggested above - the existence of two slowly fluctuating concentric ring cells in the test chamber filled with a very low Prandtl number fluid there will be pronounced "fly wheel" effects in the velocity field. The quasi rigid body rotation in such well-ordered convection cells has frequently been demonstrated by numerical simulations (see for example Clever and Busse (1981), (1987), Mundiger (1989)). Although the so far known numerical calculations are two-dimensional approaches and limited to smaller Rayleigh numbers ( $Ra < 20\,000$ ), the general features of such "fly wheel" velocity patterns are reflected in the Nusselt-Rayleigh number correlation for the heat transfer, which according to Busse and Clever (1981) should correlate for  $Ra \gg 1$  as  $Nu \sim Ra^{1/4}$ . Our measurements follow this relationship in a wide range of Rayleigh numbers  $2 \cdot 10^4 < Ra < 5 \cdot 10^6$ . Our experimental set up and consequently the observed large scale flow pattern differs from findings of other authors like Castaing et al. (1989), Sano et al. (1989), Cioni (1993), Takeshita (1996) as these experimenters work with cylindrical test chambers of aspect ratio  $d/h = 1$ .

These authors maintain the same single convection roll, which is oriented with its axis along the container diameter and which may rotate in azimuthal direction for the whole range of Rayleigh numbers. In general one may speculate, that the fluid dynamic instability modes they encounter are less numerous compared with the instabilities of our concentric ring roll system. Nevertheless, in the low Rayleigh number range and with mercury as a test fluid the overall features of the perturbations are similar, namely determined by two kinds of instabilities, the hydrodynamic fluctuating instabilities of low Prandtl number flows in a thermally stratified environment (see Busse (1972)) and the thermal instabilities of temperature boundary layers. There is a noticeable difference between the experiments in mercury and in sodium with  $Pr = 0.025$  and  $Pr \approx 0.006$  respectively. The measured heat transfer correlations  $Nu \sim R^m$  in mercury show a persistently higher power dependency namely  $m = 0.26$  ((Rossby (1969), Cioni (1983)) and

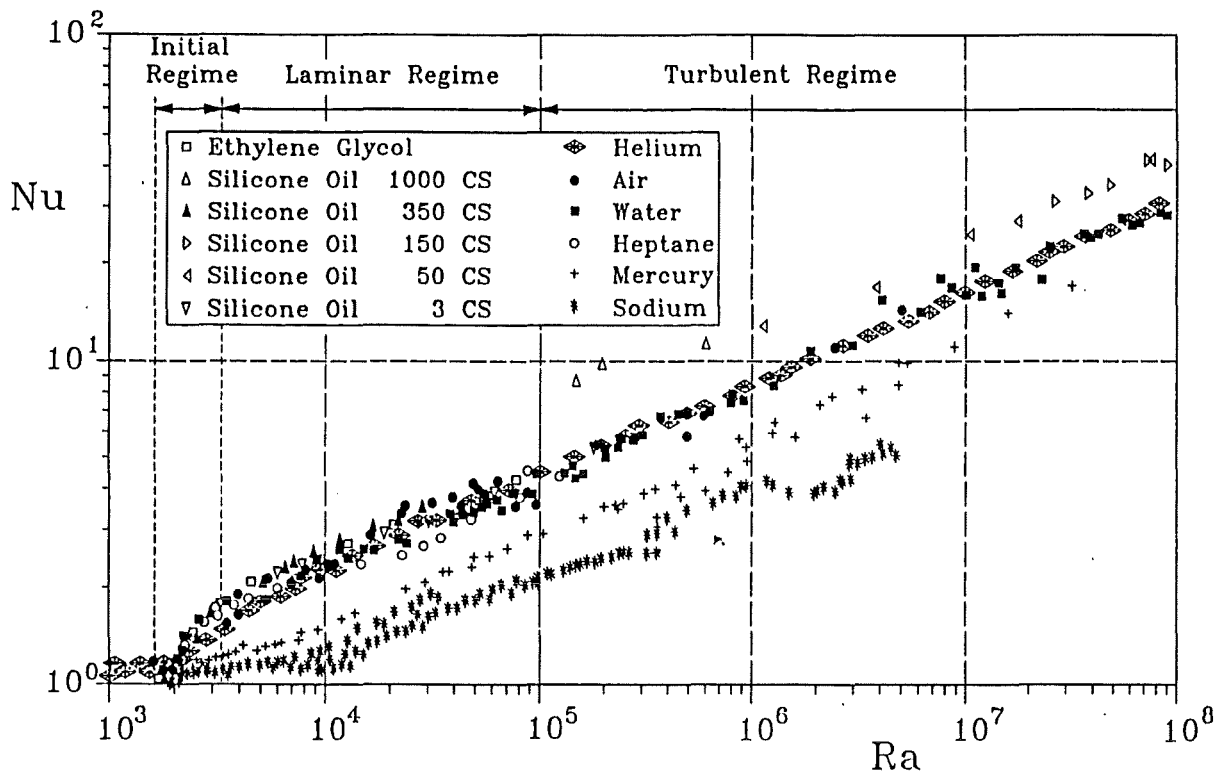


Fig. 19: Heat transfer data  $Nu(Ra)$  summarized in an O'Toole and Silveston Graph.

$m=0.286$  (Takeshita (1996)) compared with our value of  $m=0.25$ . However, the measurements were taken in different Rayleigh number ranges, for mercury in the range  $10^6 < Ra < 10^9$  and for sodium in  $10^4 < Ra < 5 \cdot 10^6$ . As the power relations reflect the different physical mechanisms of heat transport, the "mixing layer" model of Castaing et al. (1989) on the one hand and the "fly wheel" model of Jones et al. on the other hand, further experimental work is desirable to decide on the validity of the two different physical ideas.

In summary, the present available experimental data of different authors for the convective heat transfer for different fluids ranging from silicon oil to sodium and a Prandtl number varying between  $Pr \sim 10^3$  and  $\sim 10^{-3}$  are compiled in the O'Toole and Silveston (1961) graph of Fig. 19. It is quite obvious, the Nusselt number decreases at all Rayleigh numbers monotonically with the Prandtl number. There is as yet no general relationship available based on physical reasoning to describe and explain the overall correlation between the essential dimensionless groups of convective heat transfer, namely  $Nu$ ,  $Ra$  and  $Pr$ .

## Nomenclature

A	area of heat transfer	Greece symbols	
d	diameter of test cell	$\beta$	coefficient of thermal expansion
E	power density spectrum	$\Delta$	difference
F	flatness	$\varepsilon$	dissipation
h	height of test cell	$\lambda$	thermal conductivity
Nu	Nusselt number	$\kappa$	thermal diffusivity
Pr	Prandtl number	$\nu$	kinematic viscosity
PDF	probability density function	$\tau_K$	Kolmogoroff time scale
PSD	power spectrum density	$\tau_\theta$	Batchelor time scale
Ptn	resistance thermometer n	$\Phi$	correlation function
Q	electrical power		
R	radius of test cell		
Ra	Rayleigh number		
RMS	root mean square of temperature		
S	skewness		
T	mean temperature		
TC n	thermocouple n		
v	velocity		

### Subscripts:

b - Buoyancy, n - normalized, s - Signal, sod - Sodium, T - Temperature

## Figure Captions

- Fig. 1 Schematic sketch of the test apparatus; electrical power supply (1), heating plate, copper (2) sodium layer (3), side wall, nickel (4), cooling plate, copper (5), boiling cooler, oil (6), heat exchanger, water/oil (7).
- Fig. 2a Radial positions of Pt-100 resistance thermometers in the heating (H) and cooling (C) plates and of thermocouple rakes TC-rake 1 and TC-rake 2 in the sodium layer, respectively.
- Fig. 2b Axial positions of thermocouples on the TC-rake 2.
- Fig. 3 Temperature histories of the six Pt-100 thermometers each separated by  $60^\circ$  on a radial position  $r/R=0.7$ . Power supply is varied from 11 kW to 14 kW and down to 5 kW.
- Fig. 4 Schematic sketch of the flow pattern for an aspect ratio  $d/h=4.5$  of the sodium layer.
- Fig. 5a Measured local surface temperatures of heating and cooling plate.
- Fig. 5b Measured mean temperature differences between the surfaces of heating and cooling plate versus heating power
- Fig 6a Radial profiles of the mean temperature differences measured by the 6 pairs of opposite Pt-100 thermometers.
- Fig. 6b Mean temperature differences versus power supply at the positions  $r/R=0$  and  $r/R=0.7$ .
- Fig. 7a Dimensionless heat transfer correlation  $Nu(Ra)$  evaluated for the aspect ratio  $d/h=4.5$ .
- Fig. 7b: Dimensionless heat transfer correlation  $Nu(Ra)$  evaluated for the aspect ratios 33 (○○○), 11 (□□□) and 4.5 (+ + +).
- Fig. 8: Mean temperature profiles for different  $Ra$ -numbers across the sodium layer at the position of TC-rake 2.
- Fig. 9: Temperature histories recorded from thermocouples of TC-rake 2 at the axial positions: surface of heating plate (TC 10), middle of sodium layer (TC 15) and surface of cooling plate (TC 20) for  $Ra=2 \cdot 10^6$  (a),  $Ra=2.9 \cdot 10^6$  (b) and  $Ra=4.3 \cdot 10^6$  (c).
- Fig. 10: Normalized temperature histories recorded from Pt-100 thermometers at the positions  $r/R=0$  (□□□),  $r/R=0.7$  (+ + +).
- Fig. 11: RMS-profiles of thermocouple signals of TC-rake 2 across the sodium layer for different Rayleigh numbers.
- Fig. 12: RMS-values normalized by the mean temperature differences across the sodium layer versus Rayleigh number.
- Fig. 13: Normalized power spectrum density functions of TC 15 signals for the Rayleigh numbers  $Ra=4 \cdot 10^6$  (A),  $Ra=1.5 \cdot 10^6$  (B) and  $Ra=3.6 \cdot 10^5$  (C).

- Fig. 14 Signal velocity of temperature fluctuations obtained from cross-correlation of temperature signals of TC 13 and TC 17.
- Fig. 15 Normalized probability density functions of temperature signals of TC 15 (a) and TC 10 (b) for  $Ra = 4 \cdot 10^6$ . Comparison of original (○) and high pass filtered (●) data.
- Fig. 16 Normalized probability density function of temperature signal of TC 15 (original data) for  $Ra = 3.6 \cdot 10^5$ .
- Fig. 17 Normalized probability density function of temperature signal of TC 15 (original data) for  $Ra = 1.5 \cdot 10^6$ .
- Fig. 18 Profiles of skewness (a) and flatness (b) for different Ra-numbers across the sodium layer at the position of TC-rake 2.
- Fig. 19 Heat transfer data  $Nu(Ra)$  summarized in an O'Toole and Silveston Graph.

## References

- Batchelor, G. K.; Howells, I. D.; Townsend, A. A.; 1959  
Small-scale variation of convected quantities like temperature in turbulent fluid.  
The case of large conductivity  
J. Fluid Mech. 5, 134-139
- Bolgiano, R.; 1959  
Turbulent Spectra in a Stably Stratified Atmosphere  
J. Geograph. Res. 64, 2226-2228
- Bremhorst, K.; Krebs, L.; Müller, U.; Listijono, J. B. H.; 1989  
Application of a gradient diffusion and dissipation time scale model for prediction of mean and fluctuating temperature fields in liquid sodium downstream of a multi-bore jet block  
Int. J. Heat Mass Transfer 11, 2037-2046
- Busse, F.H.; 1967  
Non-stationary finite amplitude convection  
J. Fluid Mech. 28, 223-239
- Busse, F. H.; 1972  
The Oscillatory Instability of Convection Rolls in low Prandtl Number Fluid  
J. Fluid Mech. 52, 97-112
- Busse, F. H.; 1981  
An asymptotic model of two-dimensional convection in the limit of low Prandtl number  
J. Fluid Mech. 102, 75-83
- Castaing, B.; Gunaratne, G.; Heslot, F.; Kadanoff, L.; Libchaber, A.; Thomae, S.; Wu, X. Z.; Zaleski, St.; Zanetti, A.; 1989  
Scaling of hard thermal turbulence in Rayleigh-Benard convection  
J. Fluid Mech. 204, 1-30
- Chilla, H.; Ciliberto, S.; Innocenti, C.; Pampaloni, E.; 1993  
Boundary Layer and Scaling Properties in Turbulent Thermal Convection  
IL NUOVO CIMENTO 15D, 1229-1249
- Chu, T.Y.; Goldstein, R.J.; 1973  
Turbulent convection in a horizontal layer of water  
J. Fluid Mech. 60, 141-159
- Cioni, S.; 1993  
Convezione termica in fluidi metallici Tesi di Laurea  
Universita' Di Firenze
- Cioni, S.; Horanyi, S.; Krebs, L.; Müller, U.; 1997  
Temperature fluctuation properties in sodium convection,  
Physical Review E, submitted
- Cioni, S.; Ciliberto, S.; Sommeria, J.; 1996  
Experimental study of high Rayleigh number convection in mercury and water  
Dyn. Atm. Oceans 24, 117-127



- Deardorf, J.W.; Willis, G.E.; 1967  
Investigation of turbulent thermal convection between horizontal plates  
J. Fluid Mech. 28, 675-704
- Garon, A.M.; Goldstein, R.J.; 1973  
Velocity and heat transfer measurements in thermal convection  
Phys. Fluids 16, 1818-1825
- Gibson, C. H.; 1968  
Fine Structure of Scalar Fields Mixed by Turbulence II Spectral Theory  
Phys. Fluids 11, 2316-2327
- Globe, S.; Dropkin, D.; 1959  
Natural-convection Heat Transfer in Liquids Confined by two Horizontal Plates  
and Heated from below  
J. Heat Transfer, Febr. 24-28
- Goldstein, R.J.; Chu, T.Y.; 1969  
Thermal convection in a horizontal layer of air  
Prog. Heat and Mass Transfer 2, 55-75
- Goldstein, R.J.; Chiang, H.D.; See, D.L.; 1990  
High-Rayleigh number convection in a horizontal enclosure  
J. Fluid Mech. 213, 111-126
- Heslot, F.; Belmonte, A.; Libchaber, A.; 1993  
Temperature and velocity profiles of turbulent convection in water  
Phys. Rev. E, 47, R 2253-2256
- Hinze, J. O.; 1975  
Turbulence  
Mc Graw-Hill, Inc.
- Horanyi, S.; 1994  
unpublished Report-FZK
- Jones, C. A. Moore, D. R., Weiss, N. O.; 1976  
Axisymmetric convection in a cylinder  
J. Fluid Mech. 73, 353-388
- Kek, V.; 1989  
Benard-Konvektion in flüssigen Natriumschichten  
Dissertation, Universität Karlsruhe
- Kek, V.; Müller, U.; 1993  
Low Prandtl number convection in Layers heated from below  
Int. J. Heat Mass Transfer 36, 2795-2804
- Kikuchi, Y.; Shioyama, T.; Kawara, Z.; 1986  
Turbulent heat transport in a horizontal fluid layer heated internally and from  
below  
Int. J. Heat Mass Transfer 29, 451-461
- Koppermann, C.; 1983  
Geschwindigkeits- und Durchflußmessung in einphasigen Strömungen mit  
Kreuzkorrelationsverfahren  
Dissertation Universität Karlsruhe  
Fortschr.-Ber. VDI-Z 8, 63

- Koschmieder, E.L.; Pallas, S.G.; 1974  
Heat transfer through a shallow horizontal convecting Fluid Layer  
Int. J. Heat Mass Transfer 17, 991-1002
- Koster, J. N.; Müller, U.; 1984  
Oscillatory convection in vertical slots  
J. Fluid Mech. 139, 363-390
- Kraichnan, R.H.; 1962  
Turbulent Thermal convection at Arbitrary Prandtl Number  
Phys. Fluids 5, 1374-1389
- Krishnamurti, R.; 1995  
Low frequency oscillations in turbulent Rayleigh-Benard convection: Laboratory experiments  
Fluid Dyn. Res. 16, 87-108
- Lumley, J.L., 1970  
Stochastic Tools in Turbulence,  
Academic Press
- McDonald, J.; Connolly, T.J.; 1960  
Investigations of natural convection heat transfer in sodium  
J. Nucl. Sci. Engng. 8, 369-377
- Mika, C.; 1975  
Messung der Strömungsgeschwindigkeit in beheizten Kühlkanälen aus der Korrelation fluktuierender Temperatursignale  
Dissertation, Technische Universität Hannover
- O'Toole, J. L.; Silveston, P. L.; 1961  
Correlations of convective heat transfer in confined horizontal layers  
Chem. Engng. Prog. Symp. Ser. 67, 81-86
- PlotIT; 1990  
Commercial computer software publisher: Scientific Programming Enterprises
- Rosby, T.H., 1969  
A study of Benard convection with and without rotation  
J. Fluid Mech. 36, 309-335
- Salomon, T. H.; Gollub, J. P.; 1990  
Sheared Boundary Layers in Turbulent Rayleigh-Benard Convection  
Phys. Rev. Lett. 64, 2382-2385
- Sano, M.; Wu, X.Z.; Libchaber A.; 1989  
Turbulence in helium-gas free convection  
Phys. Rev. A 40, 6421-6430
- Shraiman, J.B.; Siggla, E.D.; 1990  
High transport in high-Rayleigh-number convection  
Phys. Rev. A 42, 3650-3653
- Siggia, E., 1994  
High Rayleigh Number Convection  
Ann. Rev. Fluid Mech.

- Somerscales, E.F.C.; Gazd, J.W.; 1969  
Thermal convection in high Prandtl number Liquids at high Rayleigh numbers  
Int. J. Heat Mass Transfer 12, 1491-1511
- Steinberg, V.; Ahlers, G.; Cannell, S.; 1985  
Pattern Formation and Wave-Number Selection by Rayleigh-Bénard Convection  
in a Cylindrical Container  
Physica scripta 32, 534-547
- Stork, K.; Müller, U.; 1975  
Convection in boxes: an experimental investigation in vertical cylinders and  
annuli  
J. Fluid Mech. 71, 231-240
- Takeshita, T; Segawa, T.; Glazier, J. A.; Sano, Mo; 1996  
Thermal Turbulence in Mercury  
Phys. Rev. Lett. 76, 1465-1468
- Tanaka, H.; Miyata, H.; 1980  
Turbulent natural convection in a horizontal water layer heated from below  
Int. J. Heat Mass Transfer 23, 1273-1281
- Tennekes, H.; Lumley, J. L.; 1974  
A first Course in Turbulence  
MIT Press, Cambridge
- Tilgner A.; Belmonte, A.; Libchaber, A.; 1993  
Temperature and velocity profiles of turbulent convection in water  
Phys. Rev. E 47, 2253-2256
- Willis, G.E.; Deardorf, J.W.; 1967  
Development of Short-Period Temperature Fluctuations in Thermal Convection  
Phys. Fluids 10, 931-937
- Wu, X.-Z.; Kadanoff, L.; Libchaber, A.; Masaki, S.; 1990  
Frequency Power Spectrum of Temperature Fluctuations in Free Convection  
Phys. Rev. Lett. 64, 2140-2143 distribution with increasing power level i. e. in-  
creasing Rayleigh numbers.
- Yakot, V.; 1989  
Correspondence principle for turbulence: Application to the Chicago experiments  
on high Rayleigh number Bénard convection  
Phys. Fluids A1, 175-178
- Zhao, A. X.; Moates, F. C.; Narayanan, R.; 1995  
Rayleigh convection in a closed cylinder - Experiments and a three dimensional  
model with temperature-dependent viscosity effects  
Phys. Fluids 7(7), 1576-1582